A probabilistic framework for assessing the hydrological impact of Faidherbia albida in an arid area of Senegal

D.M.L. Diongue, G. Brunetti, C. Stumpp, Frederic Do, Olivier Roupsard, Didier Orange, Waly Faye, Sidy Sow, Christophe Jourdan, Serigne Faye

Journal of Hydrology 622 (2023) 129717

Contents lists available at ScienceDirect

Journal of Hydrology

journal homepage: www.elsevier.com/locate/jhydrol

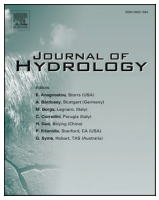

Research papers

A probabilistic framework for assessing the hydrological impact of *Faidherbia albida* in an arid area of Senegal

Djim M.L. Diongue [a], Giuseppe Brunetti [b,g,*], Christine Stumpp [b], Frederic C. Do [c,d], Olivier Roupsard [c,d,e], Didier Orange [c,d], Waly Faye [a], Sidy Sow [c,f], Christophe Jourdan [d,e], Serigne Faye [a]

[a] *Cheikh Anta Diop University of Dakar, Geology Department, Senegal*
[b] *University of Natural Resources and Life Sciences, Vienna, Department of Water, Atmosphere and Environment, Institute of Soil Physics and Rural Water Management, Muthgasse 18, 1190 Vienna, Austria*
[c] *LMI IESOL, IRD, ISRA, Bel Air, Dakar (Sénégal)*
[d] *Eco&Sols, Univ Montpellier, CIRAD, INRAE, Institut Agro, IRD, Montpellier (France)*
[e] *CIRAD, UMR Eco&Sols, Dakar, Senegal*
[f] *Gaston Berger University, UFR des Sciences Agronomiques de l'Aquaculture et des Technologies Alimentaires, Saint-Louis, Senegal*
[g] *University of Calabria, Department of Civil Engineering, Italy*

ARTICLE INFO

Keywords:
Arid areas
HYDRUS
Surrogate
Calibration
Phreatophyte

ABSTRACT

The Faidherbia tree (*Faidherbia albida*) is frequently used as an intercrop in Sahelian agroforestry parklands due to its multi-purpose advantages and reverse phenology. However, its effect upon the water balance remains unclear, due to the challenges in directly measuring water fluxes in the underlying vadose zone. Mechanistic hydrological models can be inversely calibrated on transient observations and used to partition different hydrological components, but the computational burden of the analysis can become impractical if the model itself is computationally expensive. To overcome this limitation, and to provide novel insights into the hydrological role of Faidherbia, we combine a low-fidelity, one-dimensional hydrological model (HYDRUS-1D) with a kriging-based correction function to emulate the response of a high-fidelity, two-dimensional axisymmetric description of the system (HYDRUS-2D). Multiannual measurements of soil moisture and sap flow in a Senegal agroforestry parkland are used in conjunction with Bayesian inference to calibrate the resulting validated multifidelity surrogate, and to inversely estimate soil hydraulic and root water uptake parameters. Results show that the model can reproduce observations with good accuracy and limited uncertainty for both the calibration and the validation phases, and also confirm the phreatophytic behaviour of Faidherbia by indicating the existence of a moderately compensated root water uptake. Moreover, a local sensitivity analysis suggests that a fully compensated uptake could potentially reduce groundwater recharge by 13%. Interestingly, estimated soil hydraulic parameters hint at the possibility of root-induced changes in soil hydraulic properties that mimic preferential and/or macropore flow, resulting in sustained recharge fluxes (≈ 26% of the annual precipitation). The analysis indicates that overall, Faidherbia could have a net positive effect upon the water balance in arid areas.

1. Introduction

Arid and semi-arid regions cover>40% of the Earth's land area (Koutroulis, 2019), and host about 3 billion people worldwide (Van der Esch et al., 2017). These regions are home to unique biodiversity and rich cultural heritages (Maestre et al., 2015), and provide essential ecosystem services (Bidak et al., 2015; N. Lu et al., 2018). However, the sustainable development of these areas may be seriously jeopardized by ecological issues that accrue from scarcity of water resources (e.g., lack of surface water, and low amounts of precipitation) (Kuriqi et al., 2019). In Sub-Saharan Africa (SSA), arid regions are predicted to expand due to climate change (Feng & Fu, 2013). The resulting combination of high temperatures, extremely variable rainfall, low soil fertility, and recurrent but unpredictable droughts will threaten agriculture and food production. In addition, the rapid growth of megacities increases competition for water resources (Cherlet et al., 2018). Because the

* Corresponding author.
E-mail address: giuseppe.brunetti@unical.it (G. Brunetti).

https://doi.org/10.1016/j.jhydrol.2023.129717
Received 2 January 2023; Received in revised form 3 May 2023; Accepted 20 May 2023
Available online 25 May 2023

region lacks perennial surface water, groundwater is often the only source for meeting urban, industrial, and agricultural needs (Lapworth et al., 2017; MacDonald et al., 2012). Therefore, optimal use of groundwater is crucial for SSA's development—including the region's rural economies (FAO, 1999).

Optimizing that use requires an understanding of the hydrological impact of the region's agricultural practices. One such practice is agroforestry parklands, which are widespread because of their economic, social, and environmental benefits (Mbow et al., 2014). In the agroforestry parklands of Senegal, pearl millet and groundnut are often the major crops. However, the parklands' impact upon water balance is still unclear. Jackson et al. (2005) suggest that transpiration by the parklands' large, intercropped trees is detrimental to that balance, but other studies show that the trees' roots increase groundwater recharge by altering soil hydraulic properties (Bargués Tobella et al., 2014; Ilstedt et al., 2016). The intercropped tree species *Faidherbia albida* (Del.) A. Chev. (syn. *Acacia albida* Del.) is investigated extensively in the agricultural and ecological literature (Barnes & Fagg, 2003). Its uncommon reverse phenology (shedding all of its leaves at the beginning of the rainy season (Wickens, 1969)) benefits the major crops by providing a significant nitrogen input to the topsoil at the growing season. A further benefit for the major crops is that the leafless tree canopies intercept less light and rainfall (Rhoades, 1995).

Because of these benefits, much effort has been devoted to understanding the "Faidherbia effect" upon ecosystem services and crops (Louppe et al., 1996; Tschakert et al., 2004; Roupsard et al., 2020; Leroux et al., 2020; Faye et al., 2021; T. Lu et al., 2022; Dierks et al., 2022). To understand how Faidherbia's sustains its peculiar reverse phenology in an arid region, Roupsard et al. (1999) studied the species' sap flows and water potentials, and the isotopic compositions of relevant water fractions. The results showed that Faidherbia obtains most of its water from the groundwater, thus enabling this species to grow during the dry season with little indication of drought stress. However, Faidherbia's hydrological impact remains poorly understood despite all of this scientific effort. The main difficulty lies in measuring water fluxes in the vadose zone beneath the trees. These fluxes can be inferred from other measurements, but the results frequently fail to tie together all components of the hydrological balance coherently.

An additional challenge to understanding these fluxes is the multidimensional morphological complexity of the tree roots' spatial distribution. A comprehensive theoretical framework for reproducing that complexity is offered by mechanistic vadose-zone hydrological models such as HYDRUS or SWAP (van Dam et al., 2008; Šimůnek et al., 2016). These models can discriminate the different water-balance components, but to do so, the models must describe the system's hydrologic functioning satisfactorily. Satisfactory descriptions can be generally achieved by combining data from multiple transient observations (e.g., transpiration rates and volumetric water content) with specific numerical techniques (e.g., Bayesian inference and optimization strategies) to calibrate and validate the model, and therefore to assess its predictive uncertainty (Brunetti et al., 2019a; Vrugt et al., 2008; Wöhling and Vrugt, 2011). Once the model is calibrated, it can be used to *probabilistically* separate all hydrological components (e.g., recharge and evapotranspiration fluxes), and to discern the effects of physical factors such as roots and soil.

At present, this type of approach presents multiple general and case-specific challenges. One of these challenges is that the calibration procedure requires thousands of model executions in order to assess the models' uncertainties. The computational burden of that assessment can easily become prohibitive if the model itself is computationally expensive. Modelling of fluxes in the soil-tree domain is especially susceptible to this problem because the above-mentioned morphological complexity of root systems requires a numerical model that is at least 2D axisymmetric (i.e., that has cylindrical symmetry). (See, for example, Deb et al., 2013). Supercomputers or distributed computing clusters might be able to handle the job, but are not widely available. An appealing alternative is to reduce the computational workload by using surrogate-based models in place of the complex original *high-fidelity* model (Razavi et al., 2012). When used for calibration purposes, surrogate modelling frequently aims to build an emulator that can calculate the objective function (or the likelihood) for different input parameters as if the function were being computed using the original *high-fidelity* model (e.g., a 2D axisymmetric one). Because the emulator can do the calculations in much less time, the calibration procedure is made feasible (Brunetti et al., 2017).

A diversity of water-related studies have used so-called "response-surface surrogates" successfully; including kriging, radial basis functions, and polynomial chaos expansion (Asher et al., 2015; Keating et al., 2010; Laloy et al., 2013; Razavi et al., 2012; Zeng et al., 2018; X. Zhang et al., 2009). However, when the dimensionality of the inverse problem is moderately high (e.g., >10), the necessary training of these surrogates requires an impractically high number of executions of the high-fidelity model in order to achieve a good coverage of the parameters space (O'Hagan, 2006). A possible remedy is to use *low-fidelity*, physically based surrogates, which are essentially cheaper-to-run approximations of the original complex models. For example, the surrogate model can be 1D instead of 2D (Razavi et al., 2012). When the surrogate uses the same theoretical framework and parameters as the high-fidelity model, the discrepancy between their respective response surfaces is expected to be limited. This discrepancy can be corrected by using an appropriate function that relates the responses of the low- and high-fidelity models. The so-called *multifidelity* approach develops the necessary correction function by using response-surface surrogates, which is generally easier to reconstruct because the low-fidelity response surface is supposedly a good approximation to the high-fidelity one. By thus reducing computational cost while mimicking the output of a high-fidelity forward model simulation, multifidelity surrogate analysis makes itself highly attractive for calibrating vadose zone hydrological models.

Few studies to date have calibrated vadose zone hydrological models via this approach (Man et al., 2018, 2021; Zheng et al., 2019). Therefore, the present study uses it to efficiently calibrate and validate a high-fidelity, two-dimensional axisymmetric HYDRUS model of the vadose zone underlying a Faidherbia tree in an agroforestry parkland in Senegal. The data used in the validation are from multiannual comprehensive measurements of sap flows, and of volumetric water contents at different depths. The validated multifidelity surrogate merges HYDRUS-1D and a kriging-based correction function to emulate the response of HYDRUS-2D. The surrogate is coupled with a Monte Carlo Markov Chain (MCMC) algorithm to inversely estimate soil hydraulic and root water uptake parameters, and to assess the model's predictive uncertainty. Parameters that were estimated via the surrogate are then transferred into the high-fidelity HYDRUS-2D model for validation purposes. Then, the validated HYDRUS-2D model is used to discriminate the different water fluxes; explain their interrelations; and assess their effects upon the hydrological balance. The realistic application of a multifidelity surrogate-based approach to calibrate a hydrological model of the vadose zone is a novel contribution in this field. The results can be valuable for a better understanding of water balances in agroforestry parklands in arid areas.

2. Materials and methods

2.1. Case study description and data analysis

The study area is part of the "Faidherbia-Flux" (FLUXNET/SN-Nkr) collaborative platform (https://lped.info/wikiObsSN/?Faidherbia-Flux), located in the agroforestry parkland of Sob village (135 km from Dakar) within the Senegal Groundnut basin (Roupsard et al., 2020). Soils are predominantly sandy, of a type known locally as "Dior soil" (loamy sand or Arenosols according to the USDA and FAO). The tree-based cropping system is dominated by Faidherbia albida, planted at a density of 13 trees ha^{-1}. Canopy cover is 9.6% in the main, 1-ha

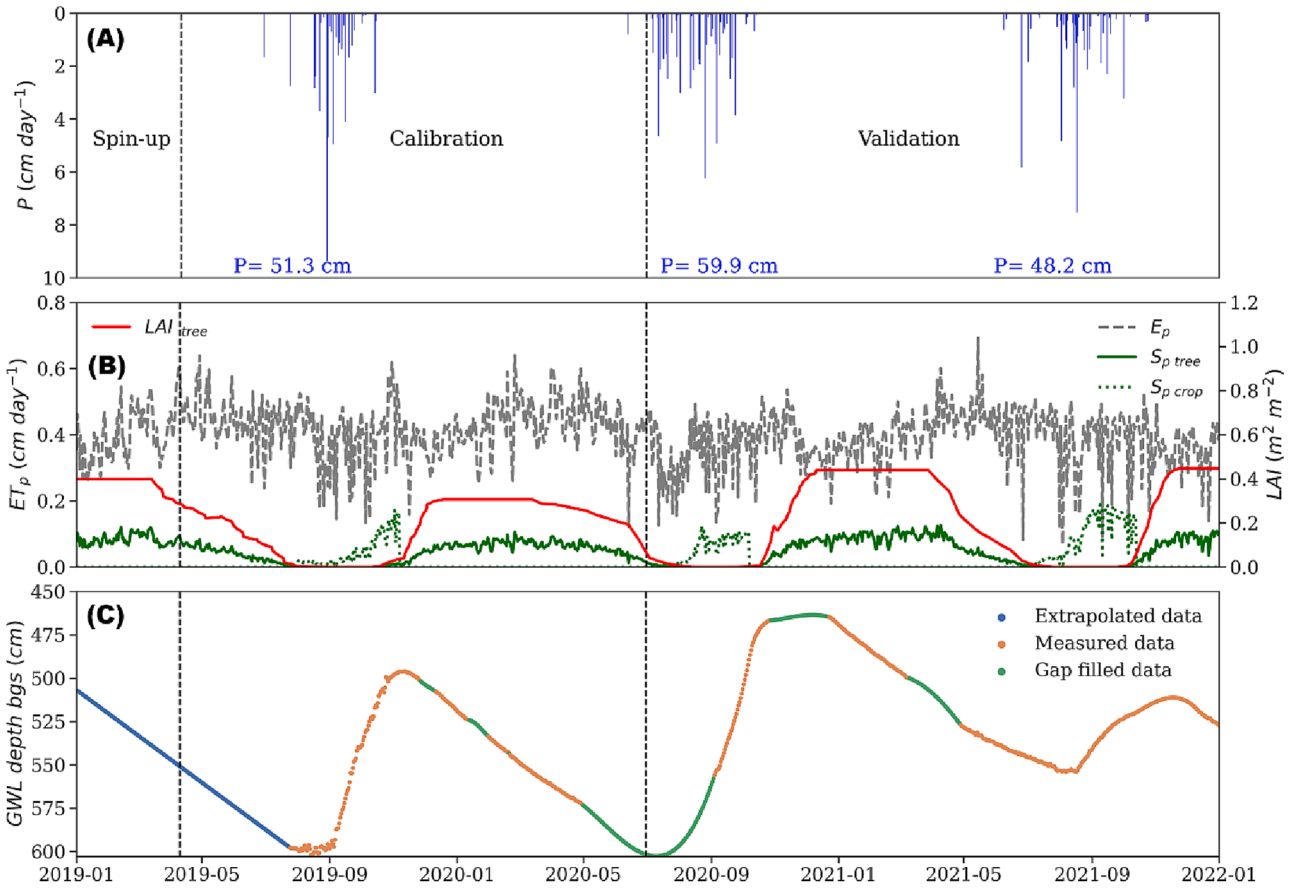

Fig. 1. Boundary conditions used for the following quantities during the three phases of modelling: (A) rainfall (P); (B) potential soil evaporation (E_p); potential crop transpiration ($S_{p\ crop}$); potential tree transpiration ($S_{p\ tree}$); tree leaf area index (LAI $_{tree}$); (C) groundwater level (GWL); and depth below the ground surface (bgs). The three phases and their respective time intervals are: spin-up (from 01 to 01-2019 to 10–04-2019), calibration (from 11 to 04-2019 to 30–06-2020), and validation (from 01 to 07-2020 to 31–12-2021).

instrumented plot. The annual crop rotation includes rainfed millet and groundnut. Climate is of Soudano-Sahelian type, with a four-month rainy season from late June to early October, and a long dry period for the rest of the year. The average temperature is 29.8 °C; reference evapotranspiration (ET_0) is 1500 mm y^{-1}; and long-term average rainfall is around 600 mm y^{-1}. The top unconfined aquifer is a Continental Terminal (CT) formation (Oligo-Miocene to Pliocene), with a shallow brackish water 4.5–6.0 m below the ground surface. This aquifer overlies an impervious Eocene marl-limestone bedrock at a depth of around 40 m.

The data that the authors used to design this research work and to validate the resulting model were collected during an intensive, three-year field experiment (from 2019 to 2021). Meteorological data were provided by an automatic station (CR1000, Campbell Sci.) equipped with classical automatic sensors that made measurements every 30 sec, and averaged them to every 30 min. Measured parameters included rainfall events (TE25MM); air temperature and relative humidity at 2 m above the ground (CS215); and wind speed at 4.5 m above ground level (Wind Master sonic anemometer (Gill Instruments, Lymington, UK). Wind speeds at 2 m were then estimated. ET_0 was computed according to the FAO-56 Penman-Monteith equation (Allen, 1998).

To estimate the amount of water used by Faidherbia trees, we neglected water storage, and assumed that the water use was equal to the transpiration, which was estimated from sap flows. These flows had been measured during 2019–2021 via the single-probe, transient-thermal-dissipation method (Do et al., 2011), with a cyclical heating of 600 sec every 30 min. The total sap flow [LT^{-1}] was calculated for each tree, and averaged between trees to yield a mean flow for an average tree of the stand. The 2019–2021 experiments also monitored the Leaf Area Indices (LAIs) of 15 Faidherbia trees, including the four whose sap flows were being measured. The LAIs were measured every 10 days, using a LAI2200 device (Li-Cor, USA) to measure transmittances.

During 2019–2021, volumetric soil–water contents were measured in shaded areas (under tree canopies) at depths of 20, 40, 60, 80, 120, 140, 160, 180, 280, and 380 cm. These data were recorded using automated time-domain reflectometers (TDR, type CS655 Campbell), which were installed horizontally in a well that was dug close to the tree. The TDRs installed at a depth $-180 < z \leq 0$ cm were locally calibrated with data on gravimetric water contents and bulk densities. The calibration procedure is explained in details in the Supplementary Material. In contrast, TDR sensors installed at a depth z < -180 cm used the factory calibration curve, which leads to an accuracy of ± 3%. Levels of the groundwater table were continuously recorded from August of 2019 by using pressure sensors (Rugged TROLL 100, coupled with Baro-TROLL 100 for barometric compensation, In-Situ, USA). The sensors were emplaced in a piezometer close to the locations of the above-mentioned TDRs. Missing data were gap-filled via cubic interpolation. A linear interpolation was used to extrapolate data back to January 2019, based upon dry-season recession curves.

Soil profiles were sampled at different depth intervals to analyse for dry bulk density and soil texture (percentages of sand, silt, and clay). Textural analyses were performed at the Institute of Soil Physics and Rural Water Management, University of Natural Resources and Life Sciences, Vienna. The sand fractions were determined by sieving; silt and clay fractions were determined via sedimentation. The analyses revealed that in the 0–100 cm depth interval, the texture was loamy

sand, with an average bulk density of 1.7 g cm^{-3}. The clay percentage was uniform at about 2.2%, but the sand percentage decreased from 85.4% at the soil surface to 77.8 % at 60 cm. In contrast, the soil from 100 down to 500 cm had a sandy-loam texture. Contents of clay (2.9–5.5%) and silt (29.3–34.7%) were higher than in the 0–100 cm layer, but the sand content was lower (67.8–59.8%).

Densities of tree root lengths were characterized underneath tree canopies and far from them, per. For this purpose, those authors excavated 1-m-square sampling pits to a depth of 1.5 m. Results showed that about 62% of Faidherbia's fine roots were distributed within the deep soil layer (100–150 cm), versus 35% in the 30–100-layer depth, and only 3% in the upper layer (0–30 cm). Interestingly, root densities in the 50–100 cm depth interval were significantly higher outside of the canopy. Although no root-density data for depths > 150 cm were investigated via excavation, field observations that were made during installation of TDRs indicate that Faidherbia roots extend far into the deep layer and the capillary fringe. This agrees with what reported in Roupsard et al. (1999).

Because we would use the above-described data set (i.e., from all of the 2019–2021 observations) to perform a multifidelity surrogate analysis, we partitioned that data into three chronological groups (one for each phase of the modelling): spin-up (from 01 to 01-2019 to 10–04-2019); calibration (11–04-2019 to 30–06-2020); and validation (01–07-2020 to 31–12-2021) (Fig. 1).

2.2. Modelling theory

2.2.1. Water flow

The variably saturated water flow in a 2D axisymmetric domain is described by the following Richards equation:

$$\frac{\partial\theta(h)}{\partial t}=\frac{1}{r}\frac{\partial}{\partial r}\left[rK(h)\frac{\partial h}{\partial r}\right]+\frac{\partial}{\partial z}\left[K(h)\left(\frac{\partial h}{\partial z}+1\right)\right]-S_a(h) \quad (1)$$

where θ is the volumetric water content [L^3L^{-3}]; h is the pressure head [L]; t is time [T], r is the radial space coordinate [L]; z is the vertical coordinate [L]; K is the unsaturated hydraulic conductivity [LT^{-1}]; and $S_a(h)$ is a sink term [$L^3L^{-3}T^{-1}$], defined as a volume of water removed from a unit volume of soil per unit of time, due to plant water uptake. By setting $r = 0$, eq. (1) reduces to the one-dimensional Richards equation. Soil hydraulic properties are parameterized via the unimodal van Genuchten-Mualem (Mualem, 1976; van Genuchten, 1980) (VGM) model, as follows:

$$\theta=\begin{cases}\frac{\theta_s-\theta_r}{(1+(\alpha|h|)^n)^m}+\theta_r \text{ if } h\le 0\\ \theta_s \text{ if } h>0\end{cases} \quad (2)$$

$$\Theta=\frac{\theta-\theta_r}{\theta_s-\theta_r} \quad (3)$$

$$K=\begin{cases}K_s\Theta^L\left[\left(1-(1-\Theta^{\frac{1}{m}})^m\right]^2 if\ h\le 0\\ K_s if\ h>0\end{cases} \quad (4)$$

$$m=1-\frac{1}{n} \quad (5)$$

where θ_r [L^3L^{-3}] is the residual soil water content; θ_s [L^3L^{-3}] is the saturated soil water content, K_s [LT^{-1}] is the saturated hydraulic conductivity; α [L^{-1}] and n [-] are empirical shape parameters; L indicates the tortuosity [-], which is frequently assumed equal to 0.5 (Mualem, 1976); and Θ is the effective saturation [-].

Compensated Root Water Uptake and Soil Water Evaporation.

The reference evapotranspiration demand is partitioned into potential transpiration (S_p) and potential soil water evaporation (E_p) using the measured LAI (Brunetti et al., 2019b; Ritchie, 1972; Sutanto et al., 2012). The following equation converts S_p to actual transpiration, S_a:

$$\frac{S_a(h)}{S_p}=\frac{1}{S_p}\int_R S_a(h,x,y,z)dxdydz=\int_R a(h,x,y,z)b(x,y,z)dxdydz=\omega \quad (6)$$

where $S_a(h,x,y,z)$ is actual root water uptake [$L^3L^{-3}T^{-1}$]; $a(h,x,y,z)$ is a dimensionless water-stress response function; $b(x,y,z)$ is a dimensionless root-density distribution function; and ω is a dimensionless water-stress index. Eq. (6) describes root water uptake for a general three-dimensional problem, but can be easily particularized for 1D vertical and 2D axisymmetric domains. Because this study models the hydrological effects of two vegetation species (i.e., Faidherbia and groundnut-millet), their effects are distinguished in the model by first specifying the root density and the potential transpiration rate for each vegetation (using the time series of LAI), and by then using eq. (6) to calculate their respective actual root water uptakes. Their sum of the two uptakes constitutes the actual sink term in eq. (1).

Based upon results from isotope methods, Roupsard et al. (1999) suggested that Faidherbia behaves mostly as a phreatophyte, but alternatively uses all root compartments along the vadose-zone profile. To account for this effect, the two models incorporate a dimensionless root adaptability factor, ω_c (which modulates the index ω that is presented in eq. (6)). ω_c is a threshold value above which any reduction in root water uptake that occurs in stressed parts of the root zone is fully compensated by an increased uptake from unstressed parts. The range of values for ω_c is $0 \le \omega_c \le 1$. Root water uptake is not compensated when $\omega_c = 1$, but is fully compensated when $\omega_c = 0$. For a detailed explanation, please see Šimůnek and Hopmans (2009).

The root water stress response (a, in eq. (6)) depends upon the soil pressure head h. To model this stress, we used Skaggs et al.'s (2006b) smooth, s-shaped function:

$$a(h)=\frac{1}{1+\left(\frac{h}{h_{50}}\right)^p} \quad (7)$$

where h_{50} is the pressure head value at which the root water uptake is reduced by 50% [L], and p is a dimensionless empirical shape parameter. The a value ranges from 0 to 1. Because actual root water uptake depends upon root density, the models include a spatially explicit root-density function ($b(x,y,z)$ in eq. (6)). This function modulates the uptake at each mesh node in the soil-domain models, and is based on the formulation proposed by Vrugt et al. (2001). Both models neglect the effect of salinity upon root water uptake, because no comprehensive measurements from the area of study are available to characterize solute distribution in the soil domain.

Potential soil water evaporation (E_p) is converted to actual evaporation (E_a) as long as the surface is sufficiently moist and the pressure head at the soil surface doesn't exceed the minimum allowed pressure head h_{Crit} [L]. This value (h_{Crit}) is estimated from the relative humidity and air temperature. However, to avoid numerical-convergence issues when solving the Richards equation, the models restrict values of h_{Crit} such that the corresponding soil water contents are at least 0.005 higher than the residual water content θ_r [L^3L^{-3}].

2.3. Model calibration and uncertainty assessment

2.3.1. Inverse estimation of soil hydraulic and root water uptake parameters

The Richards equation and the root water uptake equations [i.e., eq. (1) and (6)] include several parameters that must be defined. In the present study, we fixed the values of some of these parameters, and calibrated the others based upon the volumetric water content and sap flow observations from 2019 to 2021. Specifically, the residual water content, θ_r, is set to 0 for all soil horizons because the soil is mainly sandy (Brunetti et al., 2020). The tortuosity factor, L, is set to the common value of 0.5 (van Genuchten, 1980). For groundnut-millet, the root water uptake parameters h_{50} and p are set equal to −800 cm and 3, respectively. These values provide a good approximation to the

Table 1
Calibrated model parameters and their prior bounds; calculated means; 3%, and 97% High-Density Intervals (HDIs); and the ESS of the parameters' posterior distributions from the Bayesian analysis.

Parameter†	Parameter description	Parameter bounds	Posterior distribution			Effective Sample Size
			HDI 3%	Mean	HDI 97%	
		Soil layer (1): $0 \leq z \leq$ -100 cm				
θ_{s1} [cm^3cm^{-3}]	Saturated water content	(0.2, 0.5)	0.35	0.45	0.49	780
α_1 [cm^{-1}]	VGM shape parameter	(0.001, 0.3)	0.01	0.013	0.02	459
n_1 [-]	VGM shape parameter	(1.1, 5)	2.2	2.5	2.7	621
K_{s1} [cm day^{-1}]	Saturated hydraulic conductivity	(100, 10,000)	200	750	1,500	543
		Soil layer (2): $-100 < z \leq$ -200 cm				
θ_{s2} [cm^3cm^{-3}]	Saturated water content	(0.2, 0.5)	0.21	0.24	0.3	578
α_2 [cm^{-1}]	VGM shape parameter	(0.001, 0.3)	0.01	0.014	0.025	710
n_2 [-]	VGM shape parameter	(1.1, 5)	1.8	2.05	2.1	756
K_{s2} [cm day^{-1}]	Saturated hydraulic conductivity	(100, 10,000)	700	1,500	1,900	480
		Soil layer (3): $-200 < z \leq$ -600 cm				
θ_{s3} [cm^3cm^{-3}]	Saturated water content	(0.2, 0.5)	0.24	0.31	0.47	865
α_3 [cm^{-1}]	VGM shape parameter	(0.001, 0.3)	0.04	0.065	0.09	761
n_3 [-]	VGM shape parameter	(1.1, 5)	1.35	1.43	1.6	672
K_{s3} [cm day^{-1}]	Saturated hydraulic conductivity	(100, 10,000)	500	1,300	1,900	501
		Roots				
h_{50} (cm)	S-shaped function's parameter	(-50, −800)	−140.1	−71.8	−54.5	497
p (-)	S-shaped function's exponent	(1.01, 4)	1.1	1.3	1.6	598
ω_c (-)	Roots adaptability factor	(0, 1)	0.31	0.39	0.48	731

†The subscripts 1, 2, and 3 indicate the first, second, and third soil horizons, respectively.

piecewise linear Feddes function used by Diongue et al. (2022b) to describe the actual root water uptake of groundnut-millet. By using these assumptions, only 15 model parameters needed to be calibrated, including the saturated water content, θ_s, the VGM shape parameters, α and n, the saturated hydraulic conductivity, K_s, for three soil horizons; the root adaptability factor, ω_c; and root water uptake parameters, h_{50} and p.

2.3.2. Bayesian inference

The Bayesian inference is used to inversely estimate soil hydraulic and root water uptake parameters and to therefore assess their uncertainty. The definition of a parameters' prior distribution and a likelihood function are required to infer the parameters posterior distribution. The prior distribution is set to be bounded uniform for all parameters. Upper and lower bounds (Table 1) are chosen based on the prior information available regarding the soil textural composition, followed by a comprehensive literature review.

Selection of the likelihood functions took into consideration the types of observations that are included in the Bayesian framework, and the characteristics of each observation's measurement errors. To a large degree, those observations consisted of soil-moisture measurements. Because the final, calibrated model is intended to reproduce the deterministic part of each observed signal, the error model for each measurement should approximate the properties of the measurement's remaining stochastic part. That part depends upon the measurement device. The TDR CS655 that was used to measure soil moisture during the 2019–2021 field study determines the velocity of electromagnetic pulses as they traverse a wave-guide that is inserted into the soil. The pulses are independent of each other, thereby excluding the possibility of autocorrelation in the measurements' errors. Moreover, the procedure that was used for calibrating the TDR CS655 in the upper soil layers led to Gaussian homoscedastic residuals (Caldwell et al., 2018) with $\sigma = 0.015$ (Supplementary Material).

For these reasons, we assumed that the error residuals are uncorrelated and normally distributed, with constant variance, σ^2. Those assumptions lead to the following form for the log-likelihood function $\ell(\mathbf{u})$:

$$\ell(\mathrm{u}) = -\frac{k}{2}\ln(2\pi) - \frac{k}{2}\ln(\sigma^2) - \frac{1}{2\sigma^2}\sum_{i=1}^{k}\left(y_i(\mathrm{u}) - \tilde{y}_i\right)^2 \quad (8)$$

where k is the number of observations, $y_i(\mathbf{u})$ and $\tilde{y}_i(\mathbf{u})$ are the ith model realization and its corresponding measured value, respectively. It is worth noting that although other forms of the likelihood function [e.g., first-order autoregressive (Wöhling & Vrugt, 2011)] might improve the quality of the model's fitting, they could also compromise the objectivity of subsequent assessments of the model's adequacy. For that reason, we opted to use a traditional, measurement-motivated Gaussian likelihood function, followed by model predictive checks for both the calibration and validation period to discuss the model adequacy.

Because the calibration procedure includes sap flows, and locally and factory calibrated TDR measurements, the final log-likelihood function $L(\mathbf{u})$ is the aggregated sum of single log-likelihoods for each jth measurements set:

$$L(\mathrm{u}) = \sum_{j=1}^{3}\ell_j(\mathrm{u}) \quad (9)$$

σ are assumed equal to 0.01 cm/day for the sap flow, 0.015 and 0.03 (-) for the locally (i.e., $-180 < z \leq 0$ cm) and factory (i.e., $z <$ -180 cm) calibrated volumetric water contents, respectively.

Having selected the prior distribution and likelihood function for each of the 15 parameters, we then used a hybrid Monte Carlo Markov Chain (MCMC) ensemble sampler to estimate the parameters' posterior distributions. The algorithm combines the differential evolution snooker move developed by Ter Braak and Vrugt (2008) with the affine-invariant stretch move proposed by Goodman and Weare (2010). To improve the algorithm convergence, chains were initialized by random sampling from a multivariate normal distribution that is centred upon the global optimum, x_{opt}. This optimum was identified via the Gradient-based Comprehensive Learning Particle Swarm Optimization (G-CLPSO) that Brunetti et al. (2022) developed for the HYDRUS model. The main diagnostic for monitoring the convergence of the MCMC sampler was the Integrated Autocorrelation Time (IAT), which is the number of steps (ensemble moves) required for the chain to produce independent samples from the *true* parameter's posterior distribution. After convergence, the Python package ArViz (Kumar et al., 2016) is used to calculate further diagnostic metrics, such as the High-Density Intervals (HDIs) and the effective sample size. Further details about MCMC sampling and convergence assessment are reported in the Supplementary Material.

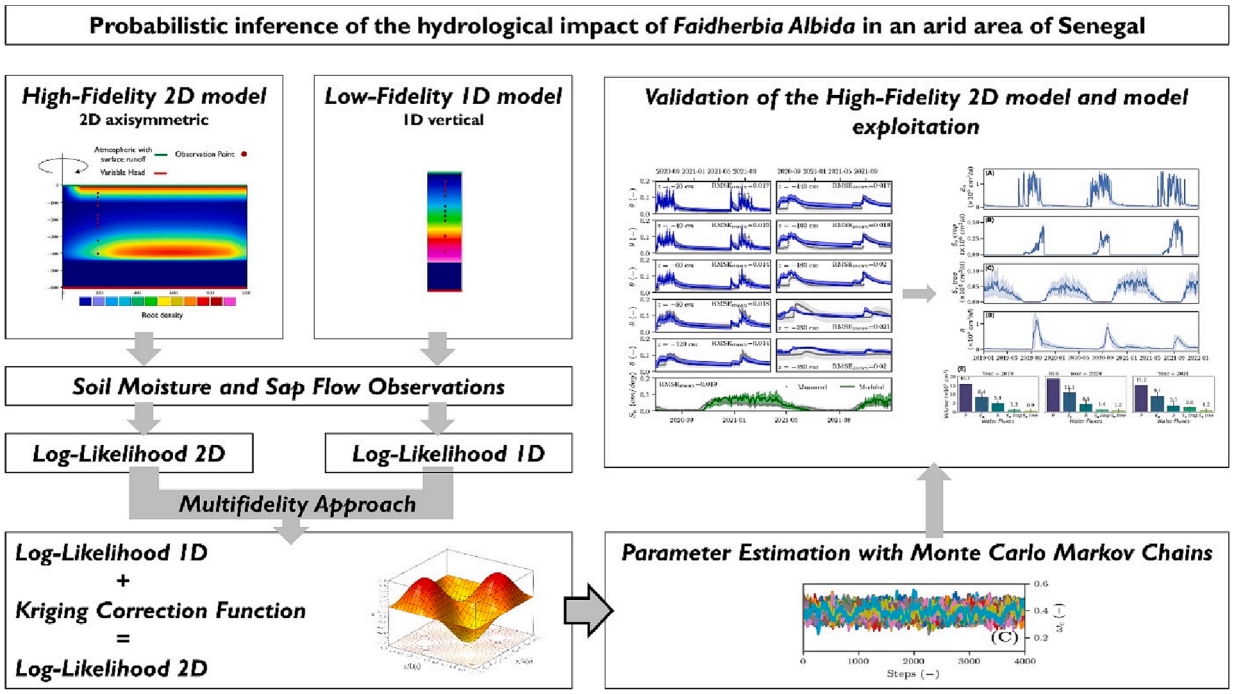

Fig. 2. A schematic of the modelling approach. The framework combines a low-fidelity *cheap-to-run* 1D model with a kriging-based correction function to approximate the log-likelihood function computed using a high-fidelity 2D axisymmetric model. The approximated log-likelihood is then used in conjunction with a Monte Carlo Markov Chain algorithm to inversely estimate soil hydraulic and root water uptake parameters, and quantify their uncertainty. Estimated parameters are then used in the high-fidelity 2D model for validation purposes and model exploitation.

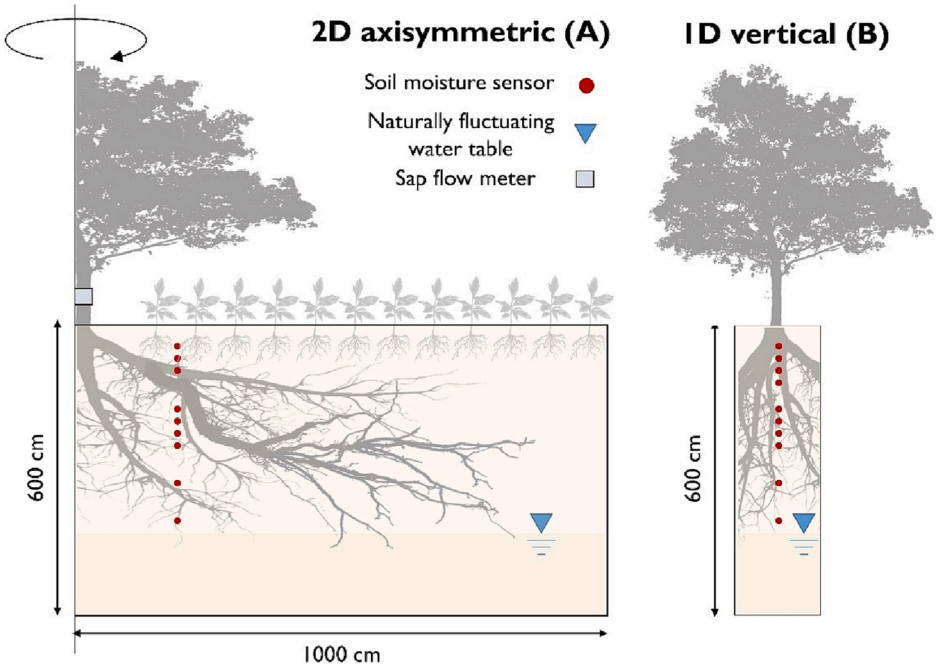

Fig. 3. Schematic of the high-fidelity axisymmetric 2D model (A) and low-fidelity 1D vertical model (B), showing also the approximate position of the naturally fluctuating water table, the position of soil moisture sensors and sap-flow meter, and the approximate distribution of roots for crops and the tree. The tree's root distribution extends beyond the dripline area; its density increases with depth until the capillary fringe.

2.4. Multifidelity surrogate analysis

2.4.1. The multifidelity approach

A schematic of the multifidelity modelling approach is shown in Fig. 2. As noted above, this study sought to produce both a high-fidelity model and a *cheap-to-run* low-fidelity model. Because our purpose was to elucidate the hydrological role of an intercropped Faidherbia tree in the underlying vadose zone, our high-fidelity model was designed to (1) reproduce field-scale observations, and (2) describe variably saturated water flows and root-water uptakes of crops as well as the tree. To overcome the lack of detailed information about root distribution, crown morphology, and soil heterogeneity, the high-fidelity model

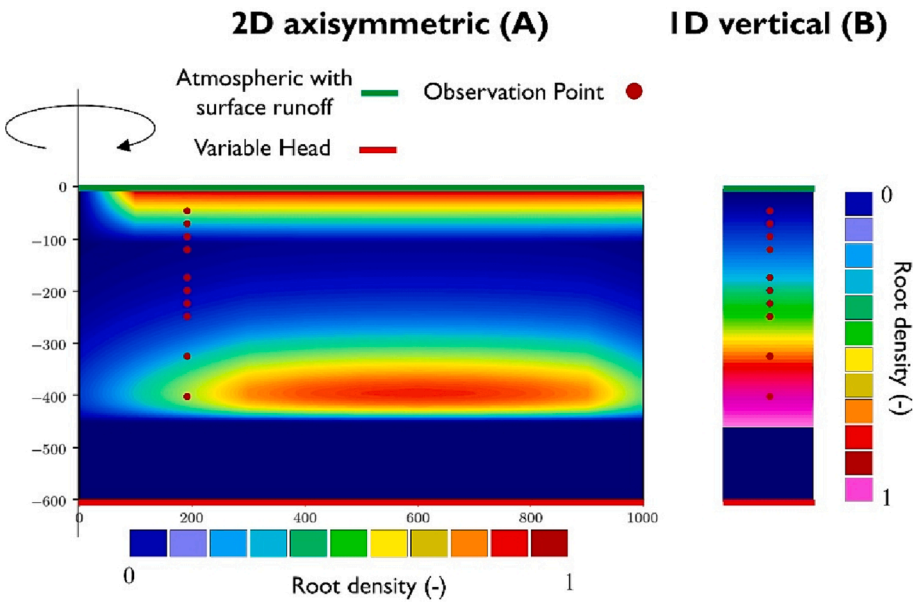

Fig. 4. Schematic of the distribution of boundary conditions for the high-fidelity axisymmetric 2D model (A) and the low-fidelity 1D vertical low-fidelity model (B). The main differences are that: (1) the spatial root distribution is simplified in 1D by assuming a linear increase with depth, and (2) the entire soil surface in 1D is assumed to be within the dripline.

assumes that these aspects of the tree-soil domain are two-dimensionally axisymmetric. Deb et al., (2013) showed that this assumption is effective and accurate. The resulting pseudo-3D discretization uses a dense 2D finite-element mesh, and allows the modeler to infer the spatial variability of water fluxes and root-water uptake [(A) in Fig. 3].

In contrast, the low-fidelity model conceptualizes processes in the soil-tree domain as strictly one-dimensional [(B) in Fig. 3]. This strong simplification of the domain's spatial variability reduces computing time, but risks biasing the calibration procedure. The present study mitigates this issue (at least partially) in two ways. We start by using the same theoretical framework for both models (high- and low-fidelity). Then, we correct the response of the low-fidelity model by using a multifidelity surrogate approach with an embedded response-surface emulator. In this way, it is possible to maximize the computational efficiency while maintaining the theoretical accuracy of the high-fidelity model.

To reduce the computational cost of the Bayesian analysis, the multifidelity approach that is used here combines the computationally efficient, low-fidelity 1D vertical model [(B) in Fig. 3 and Fig. 4] with an additive correction function to approximate the response of the computationally intensive high-fidelity, 2D axisymmetric model [(A) in Fig. 3 and Fig. 4] (Gano et al., 2006; Leary et al., 2003; Viana et al., 2009; Wu et al., 2020; J. Zhang et al., 2018). Specifically, the aggregated log-likelihood obtained from the high-fidelity model, $L_h(\mathbf{u})$, is approximated by adding a correction function, $g(\mathbf{u})$, to the aggregated log-likelihood that is calculated via the low-fidelity model, $L_l(\mathbf{u})$:

$$L_h(\mathbf{u}) = L_l(\mathbf{u}) + g(\mathbf{u}) \tag{10}$$

Because the exact form of $g(\mathbf{u})$ is unknown, an approximation to it is built by using a Gaussian process that is based on the kriging technique, which is trained on a relatively low number of high- and low-fidelity model executions. Kriging, belonging to the class of Gaussian process emulators (Rasmussen & Williams, 2006; Sacks et al., 1989), combines a polynomial model with a localized deviation model that is based upon a spatial correlation of samples:

$$g(\mathbf{u}) = f(\mathbf{u}) + Z(\mathbf{u}) \tag{11}$$

where $f(\mathbf{u})$ is a function that approximates the response surface through a set of points in the parameters' space. The vector $Z(\mathbf{u})$ is the result of a stochastic process with zero mean and nonzero covariance. The parameters in $Z(\mathbf{u})$ are optimized. For the sake of brevity, mathematical details about kriging are not reported here. Thorough theoretical descriptions of using the kriging method for surrogate analysis are given in Forrester et al. (2008) and Kennedy and O'Hagan (2001).

2.4.2. *Training and validation of the multifidelity surrogate*

The preliminary training and validation phases verify the capability of the surrogate to accurately reproduce the response of the high-fidelity model. The training/validation procedure is iterative, as described below:

The Latin hypercube sampling generates a set of parameters (McKay et al., 1979), which is used to initially train the kriging-based correction function. The training sample size, s, is set based on the relation proposed by Jones et al. (1998) [eq. (12)]:

$$s = 10D \tag{12}$$

where D is the dimensionality of the parameters' space, equal to 15 in the present study, thus leading to a total of 150 initial training sites. A *for* loop is used to iterate through the training samples, and calculate the aggregated log-likelihood [i.e., eq. (9)] for both the high and low-fidelity models and for each parameters' set.

The training set is used to optimize hyperparameters of the kriging-based correction function, and obtain a first multifidelity surrogate. The surrogate is combined with the MCMC to estimate a first approximation of the parameters posterior distribution.

The final position of the chains (i.e., 100 solutions) is used to calculate the aggregated log-likelihood for both the original high-fidelity 2D model and the multifidelity surrogate.

A dimensionless error metric, E, compares the response of the original model and the multifidelity surrogate:

$$E = \frac{\sum_{i=1}^{K} \left| L(\mathbf{u})_{high-fidelity} - L(\mathbf{u})_{multifidelity} \right|}{\sum_{i=1}^{K} \left| L(\mathbf{u})_{high-fidelity} \right|} \tag{13}$$

If the error metric is lower than 1%, it is assumed that the surrogate well approximates the response of the original model in high-likelihood regions and the validation is successful.

If the error metric is higher than 1%, the posterior solutions are

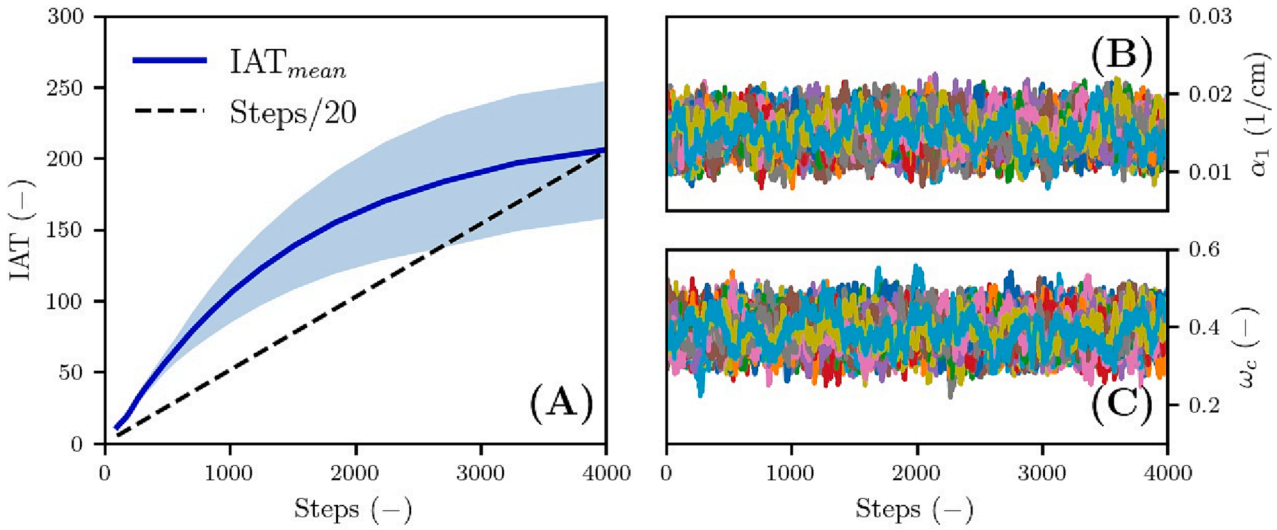

Fig. 5. Diagnostic plot of the MCMC algorithm, showing: (A) the average (blue solid line) and the standard deviation band of the integrated autocorrelation times (grey band) as a function of the number of algorithm steps. The black dashed line in (A) corresponds to the convergence threshold value of 20 IAT. (B) and (C) show the position of the chains in the ensemble as a function of the number of algorithm steps for the parameters α_1 and ω_c, respectively (each colour indicates individual runs). (A) shows that IAT is reaching its true value asymptotically, and that the length of the chains has reached the threshold value of 20 IAT. (B) and (C) complement that information by highlighting the good mixing in the ensemble and the absence of any significant trend, as confirmed by the IAT analysis.

added to training set and the process restarts from step 2.

By iteratively adding posterior solutions to the training set (*active learning*) (Zhang et al., 2020), the training procedure guarantees that the surrogate well approximates high-likelihood areas in the parameters' space. This, together with the initial well-spaced Latin hypercube sample, assures an efficient coverage of the parameters' space.

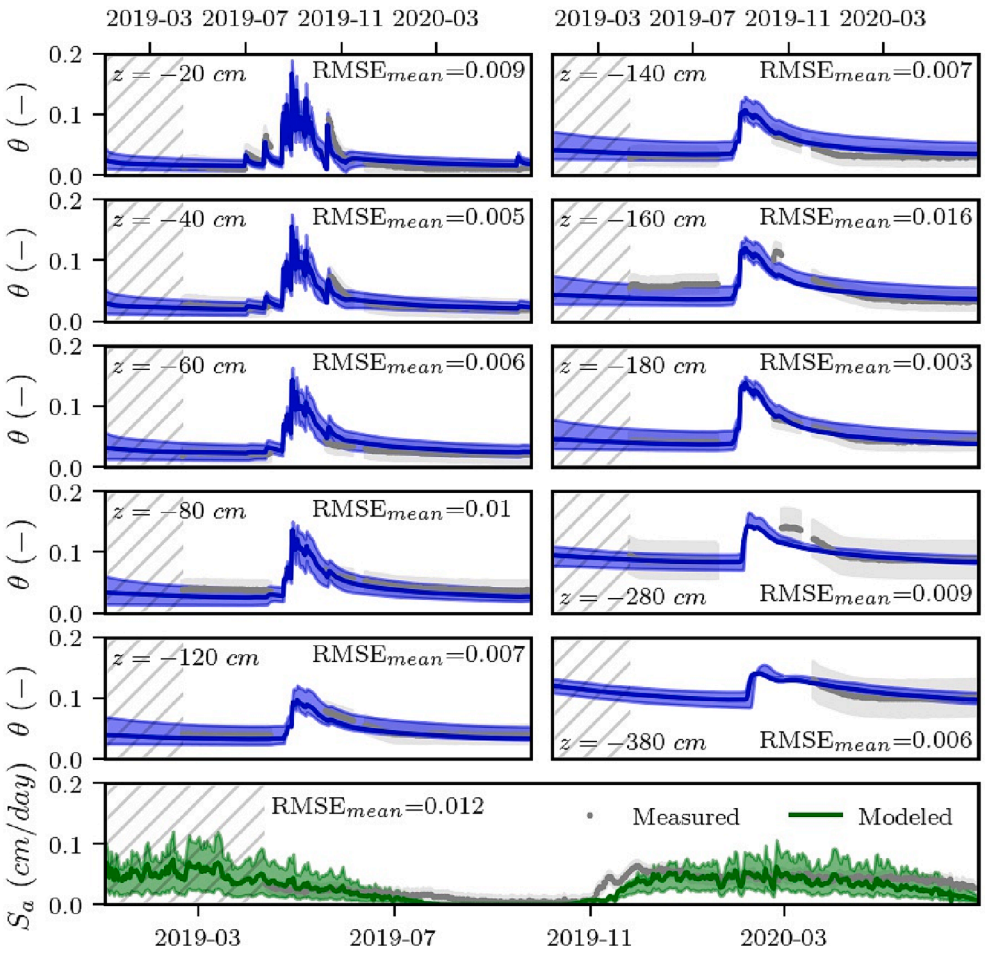

Fig. 6. Model calibration: a comparison between the model predictive uncertainty bands (blue and green areas); the mean posterior solution (solid lines); and measured values (grey circles) for sap flow (S_a) and volumetric water contents (θ) at eight different depths. Predictive bands and the mean posterior solution were obtained by propagating the calculated High-Density Interval and mean solutions (Table 1), respectively, into the high-fidelity axisymmetric HYDRUS-2D model. The hatched areas indicate the model spin-up period, while the grey bands represent the sensor accuracy. Each plot shows the RMSE that was calculated from the mean soil hydraulic and root water uptake parameters, as taken from the parameter's posterior distributions (Table 1).

2.4.3. Model setup and boundary conditions

The previously described equations for water flow and root water uptake were solved using the finite-element model, HYDRUS (Šimůnek et al., 2016). More specifically, we used a non-standard version of HYDRUS model that can simulate root water uptake from two plant species (Faidherbia and crop rotation of groundnut and pearl millet) in 2D. The high-fidelity, axisymmetric 2D domain is discretized into 4,000 2D triangular elements, and the low-fidelity 1D vertical domains is discretized into 200 1D finite elements. Both models use a finer mesh near the soil surface in order to provide accurate simulations of pressure-head gradients that are induced by atmospheric conditions. Based upon preliminary soil-texture information, both models discretize the vadose zone profile into three separate soil horizons: (1) an upper soil layer from 0 to −100 cm (i.e., to the 100 cm depth); (2) an intermediate soil layer between −100 and −200 cm; and (3) a deeper soil layer from −200 to −600 cm. In both models, the spatial distributions of the densities of crop and tree roots are constant in time. However, the spatial distributions are more detailed in the high-fidelity model than in the low-fidelity one. In particular, the high-fidelity model assumes that Faidherbia roots extend beyond the dripline area; that the root density is higher outside of the canopy; and that the root density increases with depth until the capillary fringe [(A) in Fig. 4] (Roupsard et al., 1999). At any distance from the tree, the root density of crops at the surface is assumed to increase linearly with depth, down to the maximum rooting depth of 100 cm. The simpler low-fidelity model, too, assumes that root densities of crops increase linearly with depth [(B) in Fig. 4], but also assumes that the distribution is the same for all distances from the tree.

Fig. 4 also shows the distribution of the boundary conditions (BCs) for the two models. The atmospheric boundary condition at the soil surface includes precipitation, potential soil evaporation, and potential transpiration. The pressure head at the soil surface cannot exceed (in absolute value) the minimum allowed pressure head, h_{Crit}. No flux is allowed through the vertical sides of the transport domain due to symmetry. Finally, a Dirichlet-type variable head BC is set at the bottom of the domain to simulate measured water table fluctuations.

3. Results and discussion

3.1. Model calibration

3.1.1. MCMC diagnostic

The surrogate training required, in total, 250 runs of the high-fidelity axisymmetric HYDRUS-2D model to reduce the surrogate approximation error (E) to 0.94%. The validated multifidelity surrogate was then used for the Bayesian inference via the MCMC algorithm, which required 4,000 steps, and a total of 400,000 surrogate model evaluations, to achieve the IAT convergence threshold [(A) in Fig. 5]. The mean acceptance fraction was 0.19, which is considered to be a satisfactory value if the posterior distribution is multivariate Gaussian (Gelman et al., 2004). The satisfactory performance of the sampler is further demonstrated by the good mixing of the chains in the ensemble [(B) and (C) in Fig. 5], and is proven statistically by the average ESS value (=637; Table 1).

It must be emphasized that performing 400,000 simulations with the high-fidelity axisymmetric HYDRUS-2D model would require approximately 90 days on the available computer (IntelI CITM) i7-8750H CPU 2.20 GHz, RAM 16 GB). In contrast, only four days were necessary to complete the Bayesian analysis with the multifidelity surrogate.

3.1.2. Model predictive checks

Fig. 6 shows a comparison between the model predictive uncertainty bands (blue and green areas); mean posterior solutions (solid lines); and measured values (grey circles) of sap flow (S_a) and volumetric water contents (θ) at eight different depths. The predictive bands and the mean posterior solutions were obtained by propagating the calculated High-Density Intervals (HDIs) and mean solutions, respectively (Table 1), into the high-fidelity axisymmetric HYDRUS-2D model. The results indicate that the model reproduces, with satisfactory accuracy and low predictive uncertainty, both the water distribution in the soil and the actual transpiration dynamics during the calibration period. Although the deviation between modelled and predicted volumetric water contents increases with depth, the error remains limited, as confirmed by the root mean square errors (RMSEs) calculated for the mean solution from the parameters' posterior distributions.

The predicted sap flows exhibit a time-shift error, especially during November 2019 and January 2020. Those periods coincide with the end of the rainy season and Faidherbia's re-greening period. The time shift can be partially attributed to inconsistencies between the actual sap flow and the measured LAI, which the model used to partition evapotranspiration fluxes. In particular, the underestimation of the actual sap flows may be the numerical result of the underestimated LAIs, which in turn led the model to predict low potential transpiration fluxes. We also note that the macroscopic root water uptake approach used in HYDRUS approximates the actual transpiration process only conceptually. In contrast, sap-flow measurements are a good—albeit imperfect—indicator of transpiration (Meinzer et al., 2004). Therefore, the model's time-shift error appears to be a consequence of the nature of the LAI data, rather than an indication of deficiencies in the models.

In summary, the model interpret the dynamics of Faidherbia's transpiration well, and the model predictive checks (on the whole) do not indicate significant systematic discrepancies between model predictions and observations (Gelman et al., 2004). Thus, results from the calibration phase suggest that the model can explain the underlying hydrological processes satisfactorily.

3.1.3. Assessment of the parameters

The calculated mean, and 3% and 97% High-Density Intervals (HDIs) of the parameters' posterior distributions are reported in Table 1. They indicate that the inverse problem is well-posed, with an acceptable level of uncertainty. HDIs are generally narrow, except for the saturated soil water contents (θ_s) and hydraulic conductivities (K_s), which have larger uncertainties. Those uncertainties can be partially explained by the limited range of the volumetric water contents (measured during 2019–2021), which never approached the saturated values. Thus, those measurements were mainly informative of the dry end of the retention and conductivity curves.

The relatively high estimated values of K_s might be explained by the finding of Lu et al. (2020) that in coarse soils, tree roots can increase K_s up to 1,085% by inducing the formation of macropores. Therefore, the high K_s values that we found suggest that in the area of study, macropore formation and/or preferential flow was occurring in the root zone. This behaviour was already observed by Bargués Tobella et al. (2014), who investigated the effect of scattered trees upon soil infiltrability in an agroforestry parkland in Burkina Faso. In that study, dye-tracer experiments demonstrated that preferential flow and infiltrability were significantly higher under Shea trees' canopies than in the surrounding open areas. In particular, the joint action of tree roots and high organic-matter contents from litter inputs increases the macroporosity, thus creating preferred pathways for water flow. Moreover, the potential effect of other occurring mechanisms, such as stemflow and film flow along roots (Nikodem et al., 2010), are not properly accounted in the model, but lumped in the soil hydraulic parameters. Nevertheless, the relatively high uncertainty in the estimation of K_s suggests that more specific measurements are required to better characterize the hydraulic behaviour of the system.

Overall, estimated soil hydraulic parameters are consistent with the measured soil textural composition, in that the parameters reproduce the hydraulic properties of a highly permeable sandy soil whose fine fraction increases with depth. The corresponding decrease of the coarse material is reflected in the lower value of the shape parameter, n_3, for the deeper soil layer, which contains more clay (2.9–5.5%) and silt (29.3–34.7%), but less sand (67.8–59.8). Estimated saturated water

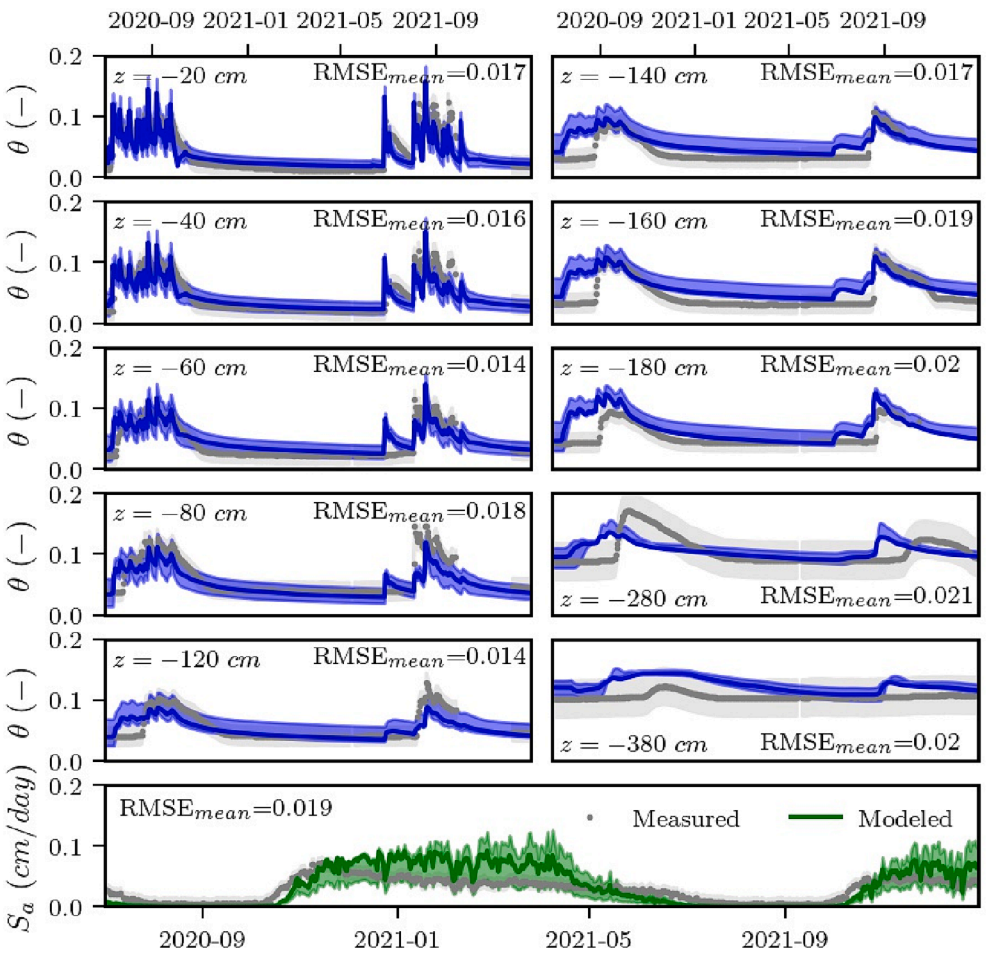

Fig. 7. Model validation: comparisons between the model predictive uncertainty bands (blue and green areas), the mean posterior solution (solid lines); and (grey circles) measured sap flow (S_a) and volumetric water contents (θ) at eight different depths. Predictive bands and the mean posterior solution were obtained by propagating the calculated High-Density Interval and mean solutions (Table 1), respectively, into the high-fidelity axisymmetric HYDRUS-2D model. Each plot shows the corresponding RMSE that was calculated by using the mean values of soil hydraulic and root water uptake parameters, as taken from the parameters' posterior distributions (Table 1).

contents (θ_s) range between 0.2 and 0.45, which would be typical for the soil that is investigated in the present study.

More interesting are the root water uptake parameters. The value of the estimated root adaptability factor, ω_c, indicates that root water uptake is moderately compensated. This finding supports the hypotheses of Roupsard et al. (1999); Roupsard et al. (2022) about the phreatophytic behaviour of Faidherbia. In particular, results from the calibration procedure indicate that roots are able to meet the transpiration demand by extracting more soil water via the less-stressed part of the roots, until ω_c reaches a value between approximately 0.31 and 0.48. At that point, the roots as a whole start to experience some stress. Deb et al. (2013) used a similar value of ω_c to simulate the compensated root water uptake of a Pecan tree. In another study, Wang et al. (2022) showed how a ω_c value between 0.3 and 0.7 led to optimal results when simulating transpiration dynamics of the phreatophyte *Tamarix ramosissima*.

The estimated pressure head at which the root water uptake is reduced by 50% (h_{50}) is relatively low (in absolute value): it ranges from −140.1 to −54.5 cm. Similar values were used by Yin et al. (2018) to simulate transpiration patterns in the phreatophyte *Salix matsudana*. Our h_{50} values, together with the estimated value of the shape parameter p, suggest that the model treats the uptake reduction as essentially a step function: under moderately wet conditions, the actual and potential transpiration are close (according to the model), but they will diverge as the pressure head increases (in absolute value) and soil pores desaturate (Skaggs et al., 2006a). This prediction is physically realistic for sandy soils (Zhu et al., 2009) like the one investigated in the present study.

It must be emphasized that because this study presents the first detailed simulation (to our knowledge) of Faidherbia's phreatophytic behaviour, it is not possible to make meaningful comparisons between our estimated root water uptake parameters and those from other existing studies on Faidherbia. However, comparisons with the existing literature on other phreatophytes, as well as the discussion about the physical meaning of the root water uptake parameters, suggest that the model provides a good approximation of Faidherbia's macroscopic behaviour of and its influence upon water fluxes in the vadose zone.

3.1.4. Model validation

To validate the high-fidelity 2D axisymmetric HYDRUS-2D model, we propagated into it the parameters' estimated posterior distributions (Table 1). Fig. 7 shows a comparison between the model-predictive-uncertainty bands (blue and green areas); the mean posterior solution (solid lines); and measured values (grey circles) of sap flow (S_a) and volumetric water contents (θ) at eight different depths. The model predictive performance generally remained satisfactory, but the bias was greater than during the calibration period. This observation is confirmed by the RMSE values that were calculated for the mean solution from the parameters' posterior distributions. Those values now range between 0.014 and 0.021 $cm^3\ cm^{-3}$ for the volumetric water content, and reach 0.019 cm day^{-1} for the sap flow. While the model approximates water distribution well in the upper soil horizons, the deviation between model predictions and measurements is greater for deeper soil layers. In particular, the model seems to systematically anticipate the arrival of the moisture front for $z <$ -100 cm, while still reproducing the peak timing and soil drying well for −100 cm $< z <$ -200 cm. This result suggests an imperfect modelling of the soil-wetting process—a deficiency that can be partially explained by the higher frequency of soil-drying data in the calibration dataset (Fig. 6). Nor is it possible to rule out possible effects of soil heterogeneity, macropore

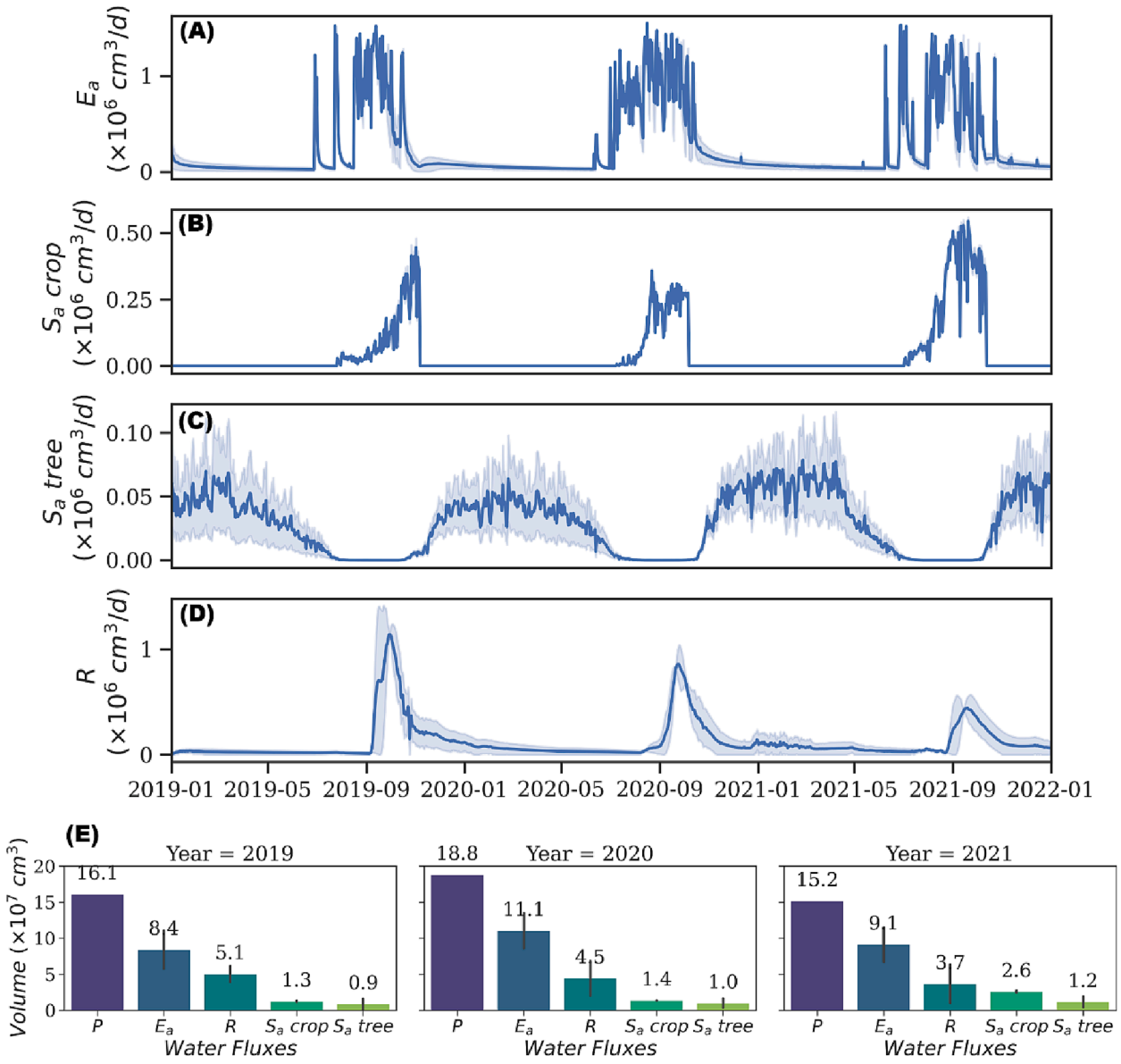

Fig. 8. Water flux partitioning as predicted by the high-fidelity axisymmetric HYDRUS-2D model: daily time series of water volume in (A) actual evaporation (E_a); (B) non-compensated root water uptake of the crops (i.e, $S_{a\ crop}$ when the roots adaptability factor $\omega_c = 1$); (C) compensated root water uptake of the tree (i.e., $S_{a\ tree}$ when the roots adaptability factor $\omega_c = 0.39$); (D) groundwater recharge (R); and (E) yearly water budget. The uncertainties of the model parameters that were derived from the Bayesian analysis are propagated into the water fluxes as the error band for the daily series and the error bar for the yearly water budget.

flow, and measurement inaccuracies. More evident is the model's overestimation of the sap flow (compared to during the calibration phase), although the transpiration pattern is again well reproduced.

The fitting could probably have been improved through a different apportioning of computation time between the calibration and validation periods (e.g., by extending the calibration and shortening the validation), as well by making the model more detailed (e.g., increasing the soil layering). However, greater detail would have increased the computational cost of the analysis by increasing both the dimensionality of the inverse problem and the complexity of the multifidelity surrogate training. Overall, results from the validation phase do not provide grounds for rejecting the model. Instead, the model's predictive performance remains satisfactory for the purpose of the analysis, which is to understand water fluxes in the vadose zone below Faidherbia trees.

3.1.5. Hydrological interpretation of water fluxes

The interpretations that follow are based upon results from the validated high-fidelity axisymmetric HYDRUS-2D model, using the parameters' estimated posterior distributions.

3.1.6. Partitioning of the water fluxes

A study of Fig. 8 shows that the model predictive uncertainty is low, except for the actual transpiration of Faidherbia ($S_{a\ tree}$) and the groundwater recharge (R). The uncertainty of these parameter is attributable to the relatively high uncertainties of the root parameters themselves.

The predicted daily actual evaporation fluxes (E_a) are low during the December-to-June dry seasons (mean: $6.6 \pm 0.4 \times 10^4$ cm^3 d^{-1}). These E_a values are representative of second-stage evaporation, during which high pressure heads at the surface limit the upward water fluxes. Conversely, the model predicts higher E_a values during the wet seasons, as expected because of the moister soil conditions. Specifically, the average predicted E_a for the wet season is $5.32 \pm 1.0 \times 10^5$ cm^3 d^{-1}, and the maximum (which occurs during rainy days) is $1.55 \pm 0.7 \times 10^6$ cm^3 d^{-1} [(A) in Fig. 8].

Wet seasons are also the times when local farmers practice the

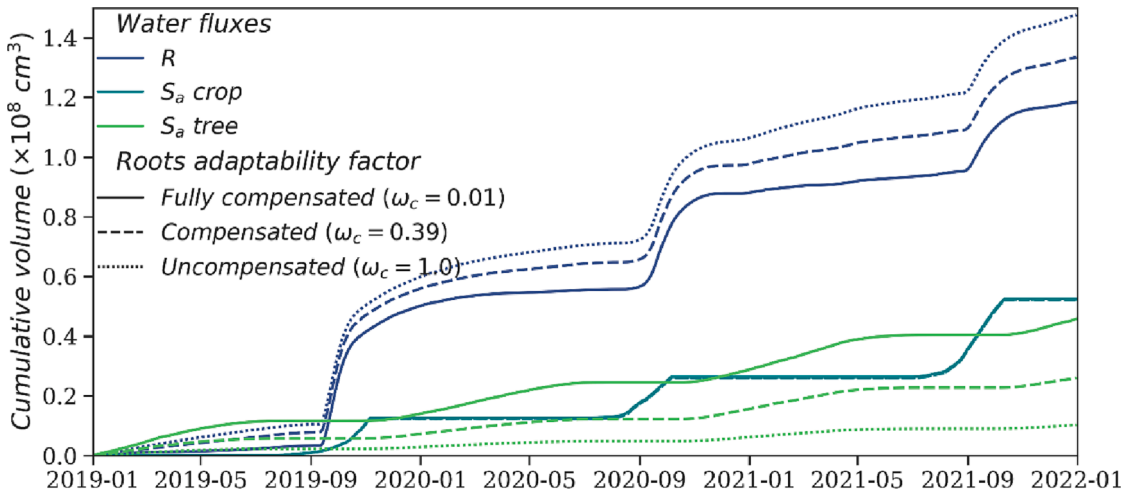

Fig. 9. (From the high-fidelity axisymmetric HYDRUS-2D model.) Time dependence of cumulative water volumes that are recharged (R), transpired by crops (S_a), and transpired by Faidherbia (*Sa* tree) when Faidherbia's root water uptake is compensated ($\omega_c = 0.39$, based on calibration results), fully compensated ($\omega_c = 0.01$), and uncompensated ($\omega_c = 1.0$).

rainfed rotation of groundnut (as they did in 2019 and 2021) and pearl millet (in 2020). The simulated daily actual transpiration of those crops, $S_{a\ crop}$, ranges from $5.7 \pm 0.0 \times 10^3$ to $8.2 \pm 1.7 \times 10^4$ cm^3 d^{-1} in the early growing stage (late July, early August), versus $1.72 \pm 0.0 \times 10^4$ to $5.4 \pm 0.02 \times 10^5$ cm^3 d^{-1} during the vegetative stage (September). Predicted values of $S_{a\ crop}$ are higher under groundnut (max: $4.95 \pm 0.45 \times 10^5$ cm^3 d^{-1}; mean: $0.52 \pm 0.03 \times 10^5$ cm^3 d^{-1}) than under pearl millet (max: $3.58 \pm 0.01 \times 10^5$ cm^3 d^{-1}; mean: $0.37 \pm 0.08 \times 10^5$ cm^3 d^{-1}). This outcome is the result of groundnut's higher LAI. The partitionings of E_a and $S_{a\ crop}$, as derived from the high-fidelity 2D model, are similar to those which Diongue et al. (2022b) computed via HYDRUS-1D for location at the study area that are outside of the trees' radius of influence (i.e., > 30 m away from any tree).

The predicted seasonal variations of Faidherbia's actual transpiration ($S_{a\ tree}$) are opposite to those of the crops, as is consistent with the species' reverse phenology. Faidherbia's predicted flux becomes negligible during the rainy season, but increases after the onset of leafing. Specifically, Faidherbia's predicted flux is around $1.48 \pm 0.56 \times 10^2$ cm^3 d^{-1} in late September and early October, and the maximums (mean: $5.17 \pm 3.75 \times 10^4$ cm^3 d^{-1}) occur during January-February. Interestingly, the onset of leafing of this phreatophyte species is paced with the groundwater recharge rate, R, (Roupsard et al., 2022), which varies from $0.44 \pm 0.15 \times 10^6$ cm^3 d^{-1} in 2021 to $1.14 \pm 0.01 \times 10^6$ cm^3 d^{-1} in 2019 [(C) and (D) in Fig. 8].

The model predicts that at the annual scale, E_a is the main component of the water balance, ranging from $8.4 \pm 2.6 \times 10^7$ cm^3 y^{-1} in 2019 (=52.3 ± 16.4% of the year's total precipitation, P) to $11.1 \pm 2.4 \times 10^7$ cm^3 y^{-1} in 2020 (=58.7 ± 13% of P). The second-largest component is R, which varied between $3.7 \pm 2.7 \times 10^7$ cm^3 y^{-1} in 2021 (=24.4 ± 17.6% of P) and $5.1 \pm 1.1 \times 10^7$ cm^3 y^{-1} in 2019 (=31.3 ± 7.1% of P) [(D) in Fig. 10]. The fluxes $S_{a\ crop}$ and $S_{a\ tree}$ are the smallest components. $S_{a\ crop}$ ranged from $1.3 \pm 0.1 \times 10^7$ cm^3 y^{-1} (7.8 ± 0.7% of P) in 2019 to $2.6 \pm 0.1 \times 10^7$ cm^3 y^{-1} (17.2 ± 1.0% of P) in 2021. $S_{a\ tree}$ was even smaller: $8.8 \pm 7.2 \times 10^6$ to $1.2 \pm 0.7 \times 10^7$ cm^3 y^{-1}, corresponding to 5.5 ± 4.5 to 7.7 ± 4.9% of P.

Groundwater recharge rates (R) predicted by the high-fidelity axisymmetric HYDRUS-2D model are higher than those which have been reported for other semiarid regions (e.g., Boumaiza et al., 2021; Gaj et al., 2016; Koeniger et al., 2016; Skrzypek et al., 2019). The predicted rates are also higher than those calculated for Senegal's Groundnut Basin by researchers who used unsaturated-zone approaches (e.g., profiles of chloride, deuterium, and tritium in soil water). For example, Edmunds and Gaye (1994); Gaye and Edmunds (1996), who studied chloride profiles at 15 separate sites and tritium profiles at two sites, showed that R averaged 5% of P in northern Senegal's Louga region, where the annual precipitation is around 290 mm y^{-1}. Similarly, Diongue et al. (2022a) found that the average R in the Groundnut Basin during 2021 was less than 2% of P, based upon stable-isotope profiles of bulk soil water.

To understand why the R values predicted by the model are higher than those from unsaturated-zone approaches, it is important to note that the latter approach postulates that none of the recharge occurs via localized (focused) paths such as tree-induced macropores. Instead, the unsaturated-zone approach assumes that all of the recharge occurs diffusely, from soil water that percolates through the vadose-zone matrix by advection-dominated flow. Therefore, the model's high R values highlight the potential impact of Faidherbia roots in generating paths for localized recharge (Bargués Tobella et al., 2014; Ilstedt et al., 2016). This impact is consistent with results reported recently by Bargués-Tobella et al. (2020). These authors, who assessed deep drainage in the openings among trees, report that deep drainage in smaller openings (where the soil is more likely to contain root-induced macropores) is>10 times higher than in openings whose centres are>22 m distant from the nearest tree trunk. Thus, Bargués-Tobella et al. (2020) highlight the decisive role that tree cover plays in promoting recharge by increasing macropore flow and deep percolation, especially near the tree trunk.

3.1.7. *Effect of root adaptability upon the water budget*

To further investigate the influence of root adaptability factors (ω_c) upon the water budget, the validated high-fidelity 2D model was used to calculate and compare $S_{a\ crop}$, $S_{a\ tree}$, and R under conditions in which Faidherbia's root water uptake (RWU) was (variously) compensated (ω_c = 0.39; a value that is based upon calibration results, and used as baseline), fully compensated (ω_c = 0.01), and uncompensated (ω_c = 1.0). The tree's cumulative transpiration (the line labelled $S_{a\ tree}$ in Fig. 9) is significantly influenced by ω_c, with values ranging from 1.03×10^7 cm^3 in uncompensated conditions to 2.60×10^7 cm^3 for compensated RWU. Transpiration remains high (4.58×10^7 cm^3) and similar to potential rates in fully compensated condition, resulting in increases of 43.2 and 77.6% compared to compensated and uncompensated root water uptake, respectively. This large increase is due to the low water-holding capacity of sandy soils, such as the one investigated in the present study. Some authors have reported that the enhanced compensated uptake occurs after significant water depletion, or after distribution of water stress over the soil profile (Deb et al., 2013; Šimůnek & Hopmans, 2009). For example, Deb et al. (2013) reported that the

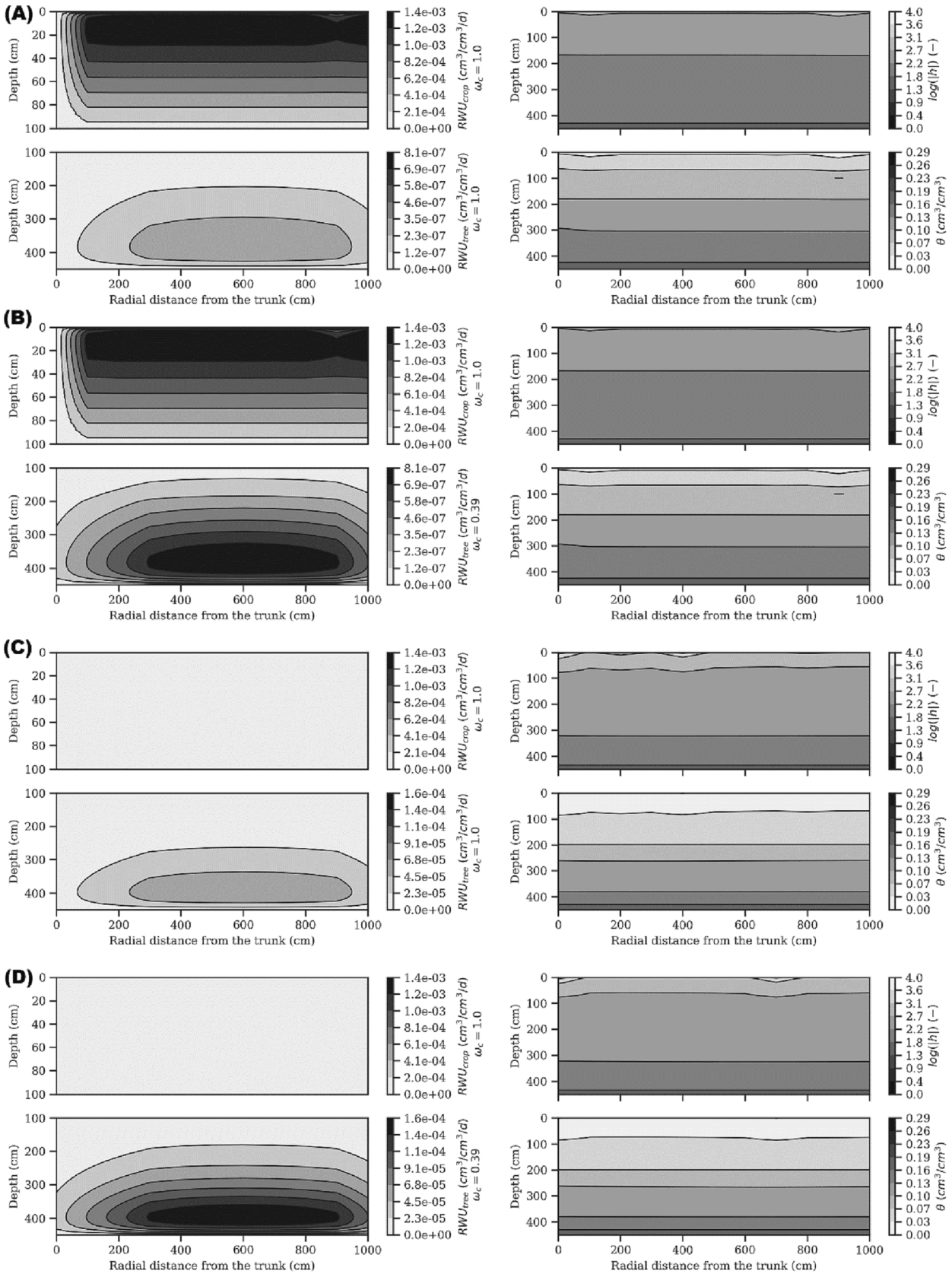

Fig. 10. Spatial-distributions of pressure head (h), soil water content (θ), and root water uptakes of the pearl millet crop and tree (RWU_{crop} and RWU_{tree}, respectively) as derived from validation of the high-fidelity axisymmetric HYDRUS-2D model. Plots in (A) and (B) are the distributions at the onset of Faidherbia's leafing (Oct. 6–10-2020). The plots in (A) show the distributions that occur without compensation ($\omega_c = 1.0$). Those in (B) show the distributions that occur with compensation for Faidherbia ($\omega_c = 0.39$). The plots in (C) and (D) are for the time of maximum leaf density (Feb, 26–02-2020). The plots in (C) show the distributions that occur without compensation ($\omega_c = 1.0$). Those in (D) show the distributions that occur with compensation for Faidherbia ($\omega_c = 0.39$).

compensated RWU of pecan trees increased by only 8% compared to the uncompensated RWU. The small magnitude of that increase was attributed to the water-holding capacity of the orchard's silty clay loam soil. Still, the increase was sufficient to avoid severe water stress during the growing season.

In the present study, the compensated RWU had no significant impact upon the crop's cumulative transpiration ($S_{a\ crop}$ in Fig. 9), which decreased by only 0.2% under fully compensated condition. This result is due to Faidherbia's reverse phenology, because of which the tree competes very little for water with adjacent crops. Conversely, increased RWU by Faidherbia in the fully compensated condition results in lower groundwater-recharge rates, with the cumulative value decreasing by 12.7% and 24.7%, respectively, compared to uncompensated and compensated RWU. This result suggests that root water uptake has an appreciable but moderate effect upon recharge fluxes. At the same time, Faidherbia can alter and potentially increase recharge fluxes through root-induce changes in the soil's hydraulic behaviour.

3.1.8. Spatial distribution of the root water uptake

To gain further insight into the strategies that Faidherbia employs to mitigate water stress, the validated model was used to investigate how the root adaptability factor (ω_c) affects spatial RWU patterns at two times of the year: during October (when Faidherbia begins its leafing, at the end of the cropping season), and in February (the time of maximum leaf density, and therefore peak transpiration demand). The 2D-contour plots in Fig. 10 show that during both periods, the compensated and uncompensated root uptakes from trees (RWU_{tree}) vary not only with soil depth, but also with radial distance from the tree trunk. The model's output also shows that in early October (6–10-2020), when pearl millet crop is in its maturity stage, then harvested a few days later, ω_c does not affect root uptake from crops (RWU_{crop}). At that time, RWU_{crop} averages 9.28×10^{-4} cm^3 cm^{-3} d^{-1}. According to results from the model, the amount of water extracted by pearl millet follows the millet's assumed root-length distribution. Specifically, RWU_{crop} is a function of depth, exclusively: at any given depth, it is the same at all distances from the tree, except within a few cm of the trunk. Moreover, RWU_{crop} is highest at the surface, and decreases linearly with depth.

During the same period (early October, 6–10-2020), Faidherbia's transpiration demand is low, and the soil is still relatively wet due to ongoing redistribution of preceding rainfall infiltration. Faidherbia roots do not experience severe water stress at this time, but extract water at higher rates in the deep layers, especially outside of the dripline area. This result is consistent with Faidherbia's root-length distribution, which is denser outside the tree canopy. The RWU_{tree} rates are minimal near the tree trunk and in the upper soil layer, but increase gradually with depth from 100 cm downward. The highest values occur within the 350–450 cm soil layer at radial distances > 300 cm. The rates decrease again in the capillary fringe. The magnitude and pattern of RWU_{tree} rates for compensated uptake (mean: 1.99×10^{-7} cm^3 cm^{-3} d^{-1}) and uncompensated uptake (0.77×10^{-7} cm^3 cm^{-3} d^{-1}) vary slightly during early October, particularly with soil depth [(A) and (B) in Fig. 10]. Indeed, to compensate the water stress, roots extract water at higher rates in the deep layers thanks to the combined effect of (1) higher root density, and (2) wetter soil and lower pressure head gradient, compared to the shallow layer.

The spatial pattern of RWU_{tree} in February differs substantially from October's due to soil drying, which is induced by the limited holding capacity of the sandy media and the higher transpiration demand of Faidherbia. In addition, roots experience more water stress in February than during October, and the magnitudes of RWU_{tree} are higher: the mean compensated RWU is 2.98×10^{-5} cm^3 cm^{-3} d^{-1}, and the mean uncompensated RWU is 1.17×10^{-5} cm^3 cm^{-3} d^{-1}. Hence, the depth distribution of RWU_{tree} is driven not only by the most densely-rooted soil layers, but also by the soil–water conditions. These hydrological behaviours of Faidherbia confirm its suitability for Sahelian agroforestry: Because of its reverse phenology, Faidherbia extracts comparatively little water throughout the cropping season, making this tree only a minor competing species (for water) with the adjacent crops. (Note that ω_c has no significant effect upon RWU_{crop}.) Furthermore, the study area's low-density stands of Faidherbia consume less than 10% of P, and use deep water to mitigate water stress.

4. Summary and conclusions

The main goal of this study was to provide further insights into the hydrological impact of Faidherbia in arid areas, by combining diverse experimental data and mechanistic modelling. To overcome the computational bottleneck, a multifidelity surrogate-based approach was adopted. The proposed surrogate merges a one-dimensional, low-fidelity description of the vadose zone beneath Faidherbia (HYDRUS-1D), with a kriging-based correction function to emulate the response of a high-fidelity, two-dimensional axisymmetric representation of the domain (HYDRUS-2D). After training and validation, a probabilistic framework based upon Bayesian inference is used to calibrate the surrogate and to inversely estimate soil hydraulic and root water uptake parameters. The comparison between model predictions and observations confirms the good predictive accuracy and limited predictive uncertainty of the model during calibration as well as validation, and thus supports the use of multifidelity surrogates as an efficient tool for reducing the computational cost of calibrating mechanistic models.

The values of the surrogate-based estimated soil hydraulic and root water uptake parameters suggest that Faidherbia induces changes in the soil hydraulic properties. These values also confirm the phreatophytic behaviour of Faidherbia. In particular, the high values calculated for the saturated hydraulic conductivities (K_s) in all soil horizons support the existence of macropore-related and/or root-induced preferential flow, which increases recharge rates significantly. This finding has been reported in other studies, but should be further investigated by performing comprehensive measurements of the root distribution and morphology, combined with tracer experiments to provide more-informative data for calibrating models. These data would make possible a robust comparison, via Bayesian modelling, in which the current unimodal Richards-based description of the water flow is tested against dual-domain or gravity-driven formulations that better describe preferential and macropore flow. By identifying the most appropriate model structure, such a comparison might confirm and assess the magnitude of these root-induced fast flows, thus further strengthening the findings of the present study, which indicates that of Faidherbia has a net positive effect upon the hydrological balance of arid areas. These detailed mechanistic analyses should be theoretically complemented by a watershed hydrological modelling to have a broader understanding of water fluxes in the agroforestry parkland.

CRediT authorship contribution statement

Djim M.L. Diongue: Conceptualization, Writing – original draft, Investigation. **Giuseppe Brunetti:** Formal analysis, Writing – original draft, Methodology. **Christine Stumpp:** Supervision, Writing – review & editing. **Frederic C. Do:** Supervision, Writing – review & editing. **Olivier Roupsard:** Supervision, Writing – review & editing. **Didier Orange:** Supervision, Investigation. **Waly Faye:** Investigation. **Sidy Sow:** Investigation. **Christophe Jourdan:** Investigation. **Serigne Faye:** Supervision, Resources.

Declaration of Competing Interest

The authors declare that they have no known competing financial interests or personal relationships that could have appeared to influence the work reported in this paper.

Data availability

Data will be made available on request.

Acknowledgments

D.M.L. Diongue received funding from CIRAD/IRD/EDEQUE, and is grateful to all Sophy's members for their warm hospitality during his stay in Vienna. Faidherbia-Flux received grants from EU-LEAP-Agri (RAMSES II), EU-DESIRA (CASSECS), EU-H2020 (SustainSahel), AGROPOLIS and TOTAL Foundations (DSCATT), CGIAR (GLDC). We are deeply grateful to the people of Sob-Niakhar, in particular I. Diouf, A. Diouf, and R. Diatte. We thank Prof. Jirka Simunek from University of California, Riverside for sharing with us the non-standard version of the HYDRUS model to simulate the effect of two vegetations. The « Laboratoire des Moyens Analytiques » (UAR IMAGO—LAMA certified ISO9001:2015), at IRD (« Institut de Recherche pour le Dévelopement ») analysed the soil samples in Dakar (http://www.imago.ird.fr/moyens-analytiques/dakar). We also thank Dr. James Smith (https://mx.linkedin.com/in/james-smith-1b195047) who revised the English.

Appendix A. Supplementary data

Supplementary data to this article can be found online at https://doi.org/10.1016/j.jhydrol.2023.129717.

References

Allen, R.G., 1998. Crop Evapotranspiration-Guideline for computing crop water requirements. Irrigation and Drain 56, 300.

Asher, M.J., Croke, B.F.W., Jakeman, A.J., Peeters, L.J.M., 2015. A review of surrogate models and their application to groundwater modeling. Water Resources Research 51 (8), 5957–5973. https://doi.org/10.1002/2015WR016967.

Bargués Tobella, A., Reese, H., Almaw, A., Bayala, J., Malmer, A., Laudon, H., Ilstedt, U., 2014. The effect of trees on preferential flow and soil infiltrability in an agroforestry parkland in semiarid Burkina Faso. Water Resources Research 50 (4), 3342–3354. https://doi.org/10.1002/2013WR015197.

Bargués-Tobella, A., Hasselquist, N.J., Bazié, H.R., Bayala, J., Laudon, H., Ilstedt, U., 2020. Trees in African drylands can promote deep soil and groundwater recharge in a future climate with more intense rainfall. Land Degradation & Development 31 (1), 81–95. https://doi.org/10.1002/ldr.3430.

Barnes, R. D., & Fagg, C. W. (2003). Faidherbia albida: monograph and annotated bibliography.

Bidak, L.M., Kamal, S.A., Halmy, M.W.A., Heneidy, S.Z., 2015. Goods and services provided by native plants in desert ecosystems: Examples from the northwestern coastal desert of Egypt. Global Ecology and Conservation 3, 433–447.

Boumaiza, L., Chesnaux, R., Drias, T., Walter, J., Stumpp, C., 2021. Using vadose-zone water stable isotope profiles for assessing groundwater recharge under different climatic conditions. Hydrological Sciences Journal 66 (10), 1597–1609. https://doi.org/10.1080/02626667.2021.1957479.

Brunetti, G., Šimůnek, J., Turco, M., Piro, P., 2017. On the use of surrogate-based modeling for the numerical analysis of Low Impact Development techniques. Journal of Hydrology 548, 263–277. https://doi.org/10.1016/j.jhydrol.2017.03.013.

Brunetti, G., Šimůnek, J., Bogena, H., Baatz, R., Huisman, J.A., Dahlke, H., Vereecken, H., 2019a. On the information content of cosmic-ray neutron data in the inverse estimation of soil hydraulic properties. Vadose Zone Journal 18 (1), 1–24.

Brunetti, G., Kodešová, R., Šimůnek, J., 2019b. Modeling the Translocation and Transformation of Chemicals in the Soil-Plant Continuum: A Dynamic Plant Uptake Module for the HYDRUS Model. Water Resources Research 55 (11), 8967–8989. https://doi.org/10.1029/2019WR025432.

Brunetti, G., Šimůnek, J., Glöckler, D., Stumpp, C., 2020. Handling model complexity with parsimony: Numerical analysis of the nitrogen turnover in a controlled aquifer model setup. Journal of Hydrology 584, 124681. https://doi.org/10.1016/j.jhydrol.2020.124681.

Brunetti, G., Stumpp, C., Šimůnek, J., 2022. Balancing exploitation and exploration: A novel hybrid global-local optimization strategy for hydrological model calibration. Environmental Modelling & Software 150, 105341. https://doi.org/10.1016/j.envsoft.2022.105341.

Caldwell, T. G., Bongiovanni, T., Cosh, M. H., Halley, C., & Young, M. H. (2018). Field and Laboratory Evaluation of the CS655 Soil Water Content Sensor. *Vadose Zone Journal*, *17*(1), 170214. https://doi.org/10.2136/vzj2017.12.0214.

Cherlet, M., Hutchinson, C., Reynolds, J., Hill, J., Sommer, S., Von Maltitz, G., 2018. World atlas of desertification rethinking land degradation and sustainable land management. Publication Office of the European Union, Luxembourg.

Deb, S.K., Shukla, M.K., Šimůnek, J., Mexal, J.G., 2013. Evaluation of Spatial and Temporal Root Water Uptake Patterns of a Flood-Irrigated Pecan Tree Using the HYDRUS (2D/3D) Model. Journal of Irrigation and Drainage Engineering 139 (8), 599–611. https://doi.org/10.1061/(asce)ir.1943-4774.0000611.

Dierks, J., Blaser-Hart, W.J., Gamper, H.A., Six, J., 2022. Mycorrhizal fungi-mediated uptake of tree-derived nitrogen by maize in smallholder farms. Nature Sustainability 5 (1), 64–70.

Diongue, D. M. L., Stumpp, C., Roupsard, O., Orange, D., Do, F. C., & Faye, S. (2022). Estimating water fluxes in the critical zone using water stable isotope approaches in the Groundnut and Ferlo basins of Senegal. https://doi.org/10.22541/au.165846607.77028000/v1.

Diongue, D.M.L., Roupsard, O., Do, F.C., Stumpp, C., Orange, D., Sow, S., Jourdan, C., Faye, S., 2022b. Evaluation of parameterisation approaches for estimating soil hydraulic parameters with HYDRUS-1D in the groundnut basin of Senegal. Hydrological Sciences Journal 67 (15), 2327–2343.

Do, F.C., Ayutthaya, I.N., S., & Rocheteau, A., 2011. Transient thermal dissipation method for xylem sap flow measurement: implementation with a single probe. Tree Physiology 31 (4), 369–380.

Edmunds, W.M., Gaye, C.B., 1994. Estimating the spatial variability of groundwater recharge in the Sahel using chloride. Journal of Hydrology 156 (1–4), 47–59.

FAO. (1999). Drylands and the MFCAL approach in cultivating our futures – Background papers prepared for The FAO/Netherlands Conference on the Multifunctional Character of Agriculture and Land (MFCAL), 12- 17 Sep 1999, Maastricht, The Netherlands. Rome, Italy: FAO.

Faye, W., Orange, D., Diongue, D. M. L., Do, F., Jourdan, C., Roupsard, O., et al. (2021). Potential impact of Faidherbia albida tree on soil infiltration in a semi-arid agroforestry system of the Senegalese groundnut basin: role of preferential flows? (No. EGU21-8768). Presented at the EGU21, Copernicus Meetings. https://doi.org/10.5194/egusphere-egu21-8768.

Feng, S., Fu, Q., 2013. Expansion of global drylands under a warming climate. Atmospheric Chemistry and Physics 13 (19), 10081–10094.

Forrester, A.I.J., Sóbester, A., Keane, A.J., 2008. Engineering Design via Surrogate Modelling: A practical Guide. J. Wiley. https://doi.org/10.1002/9780470770801.

Gaj, M., Beyer, M., Koeniger, P., Wanke, H., Hamutoko, J., Himmelsbach, T., 2016. In situ unsaturated zone water stable isotope (2H and 18O) measurements in semi-arid environments: a soil water balance. Hydrology and Earth System Sciences 20 (2), 715–731. https://doi.org/10.5194/hess-20-715-2016.

Gano, S.E., Renaud, J.E., Martin, J.D., Simpson, T.W., 2006. Update strategies for kriging models used in variable fidelity optimization. Structural and Multidisciplinary Optimization 32 (4), 287–298. https://doi.org/10.1007/s00158-006-0025-y.

Gaye, C.B., Edmunds, W.M., 1996. Groundwater recharge estimation using chloride, stable isotopes and tritium profiles in the sands of northwestern Senegal. Environmental Geology 27 (3), 246–251.

Gelman, A., Carlin, J. B., Stern, H. S., & Rubin, D. B. (2004). *Bayesian Data Analysis - Third Edition. Chapman Texts in Statistical Science Series.* https://doi.org/10.1186/1754-1611-9-2.

Goodman, J., Weare, J., 2010. Ensemble samplers with affine invariance. Communications in Applied Mathematics and Computational Science 5 (1), 65–80. https://doi.org/10.2140/camcos.2010.5.65.

Ilstedt, U., Bargués Tobella, A., Bazié, H.R., Bayala, J., Verbeeten, E., Nyberg, G., Sanou, J., Benegas, L., Murdiyarso, D., Laudon, H., Sheil, D., Malmer, A., 2016. Intermediate tree cover can maximize groundwater recharge in the seasonally dry tropics. Scientific Reports 6 (1).

Jackson, R.B., Jobbágy, E.G., Avissar, R., Roy, S.B., Barrett, D.J., Cook, C.W., Farley, K. A., le Maitre, D.C., McCarl, B.A., Murray, B.C., 2005. Atmospheric science: Trading water for carbon with biological carbon sequestration. Science 310 (5756), 1944–1947.

Jones, D.R., Schonlau, M., William, J., 1998. Efficient Global Optimization of Expensive Black-Box Functions. Journal of Global Optimization 13, 455–492. https://doi.org/10.1023/a:1008306431147.

Keating, E.H., Doherty, J., Vrugt, J.A., Kang, Q., 2010. Optimization and uncertainty assessment of strongly nonlinear groundwater models with high parameter dimensionality. Water Resources Research 46 (10). https://doi.org/10.1029/2009WR008584.

Kennedy, M. C., & O'Hagan, A. (2001). Bayesian Calibration of Computer Models. *Journal of the Royal Statistical Society. Series B (Statistical Methodology)*, *63*(3), 425–464. https://doi.org/10.1111/1467-9868.00294.

Koeniger, P., Gaj, M., Beyer, M., Himmelsbach, T., 2016. Review on soil water isotope-based groundwater recharge estimations: Review Soil Water Isotope. Hydrological Processes 30 (16), 2817–2834. https://doi.org/10.1002/hyp.10775.

Koutroulis, A.G., 2019. Dryland changes under different levels of global warming. Science of the Total Environment 655, 482–511.

Kumar, R., Carroll, C., Hartikainen, A., Martin, O., 2016. ArviZ a unified library for exploratory analysis of Bayesian models in Python Software • Review • Repository • Archive. *PyMC*. https:// 4 (33), 1143.

Kuriqi, A., Pinheiro, A.N., Sordo-Ward, A., Garrote, L., 2019. Flow regime aspects in determining environmental flows and maximising energy production at run-of-river hydropower plants. Applied Energy 256, 113980. https://doi.org/10.1016/j.apenergy.2019.113980.

Laloy, E., Rogiers, B., Vrugt, J.A., Mallants, D., Jacques, D., 2013. Efficient posterior exploration of a high-dimensional groundwater model from two-stage Markov chain Monte Carlo simulation and polynomial chaos expansion. Water Resources Research 49 (5), 2664–2682.

Lapworth, D.J., Nkhuwa, D.C.W., Okotto-Okotto, J., Pedley, S., Stuart, M.E., Tijani, M.N., Wright, J., 2017. Urban groundwater quality in sub-Saharan Africa: current status and implications for water security and public health. Hydrogeology Journal 25 (4), 1093–1116.

Leary, S.J., Bhaskar, A., Keane, A.J., 2003. A knowledge-based approach to response surface modelling in multifidelity optimization. Journal of Global Optimization 26 (3), 297–319. https://doi.org/10.1023/A:1023283917997.

Leroux, L., Falconnier, G.N., Diouf, A.A., Ndao, B., Gbodjo, J.E., Tall, L., Balde, A.A., Clermont-Dauphin, C., Bégué, A., Affholder, F., Roupsard, O., 2020. Using remote sensing to assess the effect of trees on millet yield in complex parklands of Central Senegal. Agricultural Systems 184, 102918.

Louppe, D., N'Dour, B., & Samba, A. (1996). Influence de Faidherbia albida sur l'arachide et le mil au Sénégal. Méthodologie de mesure et estimations des effets d'arbres émondés avec ou sans parcage d'animaux.

Lu, T., Brandt, M., Tong, X., Hiernaux, P., Leroux, L., Ndao, B., Fensholt, R., 2022. Mapping the abundance of multipurpose agroforestry Faidherbia albida trees in Senegal. Remote Sensing 14 (3), 662.

Lu, N., Wang, M., Ning, B., Yu, D., Fu, B., 2018. Research advances in ecosystem services in drylands under global environmental changes. Current Opinion in Environmental Sustainability 33, 92–98.

Lu, J., Zhang, Q., Werner, A.D., Li, Y., Jiang, S., Tan, Z., 2020. Root-induced changes of soil hydraulic properties – A review. Journal of Hydrology 589, 125203. https://doi.org/10.1016/j.jhydrol.2020.125203.

MacDonald, A.M., Bonsor, H.C., Dochartaigh, B.É.Ó., Taylor, R.G., 2012. Quantitative maps of groundwater resources in Africa. Environmental Research Letters 7 (2), 024009.

Maestre, F.T., Delgado-Baquerizo, M., Jeffries, T.C., Eldridge, D.J., Ochoa, V., Gozalo, B., Quero, J.L., García-Gómez, M., Gallardo, A., Ulrich, W., Bowker, M.A., Arredondo, T., Barraza-Zepeda, C., Bran, D., Florentino, A., Gaitán, J., Gutiérrez, J. R., Huber-Sannwald, E., Jankju, M., Mau, R.L., Miriti, M., Naseri, K., Ospina, A., Stavi, I., Wang, D., Woods, N.N., Yuan, X., Zaady, E., Singh, B.K., 2015. Increasing aridity reduces soil microbial diversity and abundance in global drylands. Proceedings of the National Academy of Sciences 112 (51), 15684–15689.

Man, J., Zhang, J., Wu, L., Zeng, L., 2018. ANOVA-based multi-fidelity probabilistic collocation method for uncertainty quantification. Advances in Water Resources 122, 176–186. https://doi.org/10.1016/j.advwatres.2018.10.012.

Man, J., Lin, G., Yao, Y., Zeng, L., 2021. A generalized multi-fidelity simulation method using sparse polynomial chaos expansion. Journal of Computational and Applied Mathematics 397, 113613. https://doi.org/10.1016/j.cam.2021.113613.

Mbow, C., Van Noordwijk, M., Luedeling, E., Neufeldt, H., Minang, P.A., Kowero, G., 2014. Agroforestry solutions to address food security and climate change challenges in Africa. Current Opinion in Environmental Sustainability 6, 61–67.

McKay, M.D., Beckman, R.J., Conover, W.J., 1979. Comparison of Three Methods for Selecting Values of Input Variables in the Analysis of Output from a Computer Code. Technometrics 21 (2), 239–245. https://doi.org/10.1080/00401706.1979.10489755.

Meinzer, F.C., James, S.A., Goldstein, G., 2004. Dynamics of transpiration, sap flow and use of stored water in tropical forest canopy trees. Tree Physiology 24 (8), 901–909. https://doi.org/10.1093/treephys/24.8.901.

Mualem, Y., 1976. A new model for predicting the hydraulic conductivity of unsaturated porous media. Water Resour. Res. 12, 513–522. https://doi.org/10.1029/WR012i003p00513.

Nikodem, A., Kodešová, R., Drábek, O., Bubeníčková, L., Borůvka, L., Pavlů, L., Tejnecký, V., 2010. A Numerical Study of the Impact of Precipitation Redistribution in a Beech Forest Canopy on Water and Aluminum Transport in a Podzol. Vadose Zo. J 9, 238–251. https://doi.org/10.2136/vzj2009.0083.

O'Hagan, A., 2006. Bayesian analysis of computer code outputs: A tutorial. Reliability Engineering and System Safety 91 (10–11), 1290–1300. https://doi.org/10.1016/j.ress.2005.11.025.

Rasmussen, C.E., Williams, C.K.I., 2006. Gaussian processes for machine learning. MIT Press, Cambridge, MA.

Razavi, S., Tolson, B.A., Burn, D.H., 2012. Review of surrogate modeling in water resources. Water Resources Research 48 (7), n/a-n/a. https://doi.org/10.1029/2011WR011527.

Rhoades, C., 1995. Seasonal pattern of nitrogen mineralization and soil moisture beneath Faidherbia albida (synAcacia albida) in central malawi. Agroforestry Systems 29 (2), 133–145.

Ritchie, J.T., 1972. Model for predicting evaporation from a row crop with incomplete cover. Water Resources Research 8 (5), 1204–1213. https://doi.org/10.1029/WR008i005p01204.

Roupsard, O., Audebert, A., Ndour, A.P., Clermont-Dauphin, C., Agbohessou, Y., Sanou, J., Koala, J., Faye, E., Sambakhe, D., Jourdan, C., le Maire, G., Tall, L., Sanogo, D., Seghieri, J., Cournac, L., Leroux, L., 2020. How far does the tree affect the crop in agroforestry? New spatial analysis methods in a Faidherbia parkland. Agriculture, Ecosystems & Environment 296, 106928.

Roupsard, Olivier, Faye, W., Sow, S., Diongue, D. M. L., Orange, D., Do, F. C., et al. (2022). Inverted phenology of #Faidherbia albida# paced with the dynamics of the water table (p. 1 p.). Presented at the Congrès mondial d'agroforesterie, public: Université de Laval. Retrieved from https://www.agroforestry2022.org/fr; https://conferium.com/Clients/226_web/index.lasso?lang=fr.

Roupsard, O., Ferhi, A., Granier, A., Pallo, F., Depommier, D., Mallet, B., Joly, H.I., Dreyer, E., 1999. Reverse phenology and dry-season water uptake by *Faidherbia albida* (Del.) A. Chev. in an agroforestry parkland of Sudanese west Africa. Functional Ecology 13 (4), 460–472.

Sacks, J., Welch, W. J., Mitchell, T. J., & Wynn, H. P. (1989). Design and analysis of computer experiments. *Statistical Science*, *4*(4), 409–435. https://doi.org/doi: 10.1214/ss/1177012413.

Šimůnek, J., Hopmans, J.W., 2009. Modeling compensated root water and nutrient uptake. Ecological Modelling 220 (4), 505–521.

Šimůnek, J., van Genuchten, M.T., Šejna, M., 2016. Recent Developments and Applications of the HYDRUS Computer Software Packages. Vadose Zone Journal 15 (7), 25. https://doi.org/10.2136/vzj2016.04.0033.

Skaggs, T.H., Shouse, P.J., Poss, J.A., 2006a. Irrigating Forage Crops with Saline Waters: 2. Modeling Root Uptake and Drainage. Vadose Zone Journal 5 (3), 824–837. https://doi.org/10.2136/vzj2005.0120.

Skaggs, T.H., van Genuchten, M.T., Shouse, P.J., Poss, J.A., 2006b. Macroscopic approaches to root water uptake as a function of water and salinity stress. Agricultural Water Management 86 (1–2), 140–149. https://doi.org/10.1016/j.agwat.2006.06.005.

Skrzypek, G., Dogramaci, S., Page, G.F.M., Rouillard, A., Grierson, P.F., 2019. Unique stable isotope signatures of large cyclonic events as a tracer of soil moisture dynamics in the semiarid subtropics. Journal of Hydrology 578, 124124. https://doi.org/10.1016/j.jhydrol.2019.124124.

Sutanto, S.J., Wenninger, J., Coenders-Gerrits, A.M.J., Uhlenbrook, S., 2012. Partitioning of evaporation into transpiration, soil evaporation and interception: A comparison between isotope measurements and a HYDRUS-1D model. Hydrology and Earth System Sciences 16 (8), 2605–2616. https://doi.org/10.5194/hess-16-2605-2012.

Ter Braak, C.J.F., Vrugt, J.A., 2008. Differential Evolution Markov Chain with snooker updater and fewer chains. Statistics and Computing 18 (4), 435–446. https://doi.org/10.1007/s11222-008-9104-9.

Tschakert, P., Khouma, M., Sène, M., 2004. Biophysical potential for soil carbon sequestration in agricultural systems of the Old Peanut Basin of Senegal. Journal of Arid Environments 59 (3), 511–533. https://doi.org/10.1016/j.jaridenv.2004.03.026.

van Dam, J.C., Groenendijk, P., Hendriks, R.F., a., & Kroes, J. G, 2008. Advances of Modeling Water Flow in Variably Saturated Soils with SWAP. Vadose Zone Journal 7 (2), 640. https://doi.org/10.2136/vzj2007.0060.

Van der Esch, S., Ten Brink, B., Stehfest, E., Sewell, A., Bouwman, A., Meijer, J., et al., 2017. Exploring the impact of changes in land use and land condition on food, water, climate change mitigation and biodiversity: Scenarios for the UNCCD Global Land Outlook. The Hague.

van Genuchten, M.T., 1980. A Closed-form Equation for Predicting the Hydraulic Conductivity of Unsaturated Soils1. Soil Science Society of America Journal 44 (5), 892–898. https://doi.org/10.2136/sssaj1980.03615995004400050002x.

Viana, F.A.C., Steffen, V., Butkewitsch, S., De Freitas Leal, M., 2009. Optimization of aircraft structural components by using nature-inspired algorithms and multi-fidelity approximations. Journal of Global Optimization 45 (3), 427–449. https://doi.org/10.1007/s10898-008-9383-x.

Vrugt, J.A., Hopmans, J.W., Šimunek, J., 2001. Calibration of a Two-Dimensional Root Water Uptake Model. Soil Science Society of America Journal 65 (4), 1027–1037. https://doi.org/10.2136/sssaj2001.6541027x.

Vrugt, J.A., Stauffer, P.H., Wöhling, T.h., Robinson, B.A., Vesselinov, V.V., 2008. Inverse Modeling of Subsurface Flow and Transport Properties: A Review with New Developments. Vadose Zone Journal 7 (2), 843–864.

Wang, T., Wang, P., Wu, Z., Yu, J., Pozdniakov, S.P., Guan, X., Wang, H., Xu, H., Yan, D., 2022. Modeling revealed the effect of root dynamics on the water adaptability of phreatophytes. Agricultural and Forest Meteorology 320, 108959.

Wickens, G.E., 1969. A study of Acacia albida Del. (Mimosoideae). Kew Bulletin 23 (2), 181.

Wöhling, T., Vrugt, J.A., 2011. Multiresponse multilayer vadose zone model calibration using Markov chain Monte Carlo simulation and field water retention data. Water Resources Research 47 (4). https://doi.org/10.1029/2010WR009265.

Wu, W., Ren, J., Zhou, X., Wang, J., Guo, M., 2020. Identification of source information for sudden water pollution incidents in rivers and lakes based on variable-fidelity surrogate-DREAM optimization. Environmental Modelling and Software 133, 104811. https://doi.org/10.1016/j.envsoft.2020.104811.

Yin, L., Zhou, Y., Xu, D., Zhang, J., Wang, X., Ma, H., Dong, J., 2018. Response of phreatophytes to short-term groundwater pumping in a semiarid region: Field experiments and numerical simulations. Ecohydrology 11 (4), e1948.

Zeng, X., Ye, M., Wu, J., Wang, D., Zhu, X., 2018. Improved Nested Sampling and Surrogate-Enabled Comparison With Other Marginal Likelihood Estimators. Water Resources Research 54 (2), 797–826.

Zhang, J., Man, J., Lin, G., Wu, L., Zeng, L., 2018. Inverse Modeling of Hydrologic Systems with Adaptive Multifidelity Markov Chain Monte Carlo Simulations. Water Resources Research 54 (7), 4867–4886. https://doi.org/10.1029/2018WR022658.

Zhang, X., Srinivasan, R., Van Liew, M., 2009. Approximating SWAT Model Using Artificial Neural Network and Support Vector Machine. JAWRA Journal of the American Water Resources Association 45 (2), 460–474. https://doi.org/10.1111/j.1752-1688.2009.00302.x.

Zhang, J., Zheng, Q., Chen, D., Wu, L., Zeng, L., 2020. Surrogate-Based Bayesian Inverse Modeling of the Hydrological System: An Adaptive Approach Considering Surrogate Approximation Error. Water Resour. Res. 56, e2019WR025721 https://doi.org/10.1029/2019WR025721.

Zheng, Q., Zhang, J., Xu, W., Wu, L., Zeng, L., 2019. Adaptive Multifidelity Data Assimilation for Nonlinear Subsurface Flow Problems. Water Resources Research 55 (1), 203–217. https://doi.org/10.1029/2018WR023615.

Zhu, Y., Ren, L., Skaggs, T.H., Lü, H., Yu, Z., Wu, Y., Fang, X., 2009. Simulation of *Populus euphratica* root uptake of groundwater in an arid woodland of the Ejina Basin. China. *Hydrological Processes* 23 (17), 2460–2469. https://doi.org/10.1002/hyp.7353.